Analytical Descriptions of High-T$_c$ Cuprates by Introducing Rotating Holes and a New Model to Handle Many-Body Interactions

Shinichi Ishiguri

Nihon University, 1-2-1 Izumi-Cho, Narashinoshi, Chiba 275-8575 Japan; shinichi.ishiguri@gmail.com

Abstract: This study describes the properties of high-T$_c$ cuprates by introducing rotating holes that are created by angular momentum conservations on a 2D CuO$_2$ surface, and which have a different mass from that of a normal hole because of the magnetic field energy induced by the rotation. This new particle called a macroscopic Boson describes the doping dependences of pseudo-gap temperature and the transition temperature at which an anomaly metal phase appears and describes the origin of the pseudo-gap. Furthermore, this study introduces a new model to handle many-body interactions, which results in a new statistic equation. This statistic equation describing many-body interactions accurately explains why high-T$_c$ cuprates have significantly high critical temperatures. Moreover, a partition function of macroscopic Bosons describes the properties of anomaly metal phase, which sufficiently agree with experiments. Note that, the calculations were conducted, using the result from our previous study that analytically describes the doping dependence of T$_c$. By introducing a macroscopic Boson and the new statistical model for many-body interactions, this study uncovered the mystery of high-T$_c$ cuprates, which have been a challenge for many researchers. An important point is that, in this study, pure analytical calculations are consistently conducted, which agree with experimental data well (i.e., they do not use numerical calculations or fitting methods but use many actual physical constants).

Keywords: high-T$_c$ cuprates; macroscopic Boson; many-body interactions; pseudo-gap; critical temperature; anomaly metal phase; conservation of angular momentum; attractive force; cooper pair

Introduction

First of all, note that, as the abstract mentioned, the present paper is written under the condition that our previously published article [1] was understood that describes the T$_c$-formula analytically. However, the present paper will provide the review sections.

Although several significant advancements have been presented, from the initial discovery of a superconductor, the most impressive discoveries are CuO$_2$-based superconductors (i.e., high-T$_c$ cuprates) [2]. This is because, prior to this result, superconductors generally require significantly high refrigeration because of their lower critical temperature (~20 K). However, because high-T$_c$ cuprates have higher T$_c$ than LN$_2$, they received considerable attention and interests from condensed matter physics researchers and researchers in technologies. They demonstrated interest in the technical merits when applied to superconducting magnetic energy storage and energy transmission [3–5]. Thus, initial results demonstrated that high-T$_c$ cuprates involved researchers from many condensed matter physics and related technologies.

However, condensed matter physics researchers investigated high-T$_c$ cuprates for much deeper reasons, i.e., they are the first case at which the standard band model and the Bardeen–Cooper–Schieffer (BCS) theory are not applied, which indicates that novel physical phenomena occurred. (Recent H-based superconductors [6–9] with extremely high pressures have high potentials to be applied to the BCS theory.) Note that it was considered that BCS theory could be applied to materials whose critical temperatures are up to around 30 K. Furthermore, crucially while BCS theory exhibits

isotope effects, it was found that, in high-T_c cuprates, the normal isotope effects were not applied. Considering these facts, it is clear that the mechanism of the high-T_c cuprates differs from that of BCS theory, which gave this paper a motivation to make the mechanism be clear. Moreover, it is obvious that, similar to the BCS theory, the use of quantum field theory is not adequate because quantum field theory is extremely abstract and does not reflect the fact that a phenomenon in condensed matter physics involves many actual physical constants.

Furthermore, many claimed that it is related to many-body interactions [10], which made many theoretical researchers' approaches to the mechanism difficult. Thus, it is necessary to consider the mechanism of the cuprates with many-body interactions.

Moreover, while all researchers agree that the carrier is a Cooper pair, the origin is still unclear. Although multiple theories exist discussing the nature of the force to combine a Cooper pair and the origin of pseudo-gap using RVB model or Hubbard-like model, few theoretical articles analytically address and explain experiments data, in addition to the anomaly metal phase and the transition temperature T_0 at which the anomaly metal phase appears. Thus, our paper needs to make clear the origin of attractive force to provide a Cooper pair.

Currently, there are many theories besides BCS theory. Here, let us consider why these existing theories are insufficient: Although many studies about the experiments have been reported [11–16], (in particular, STM and STS [17,18] experimental methods to date revealed many aspects in high-T_c cuprates,), no theory describes all of the experimental data.

These theories are divided to two methods: either Fermi-liquid model or resonating valence bond (RVB) model [19–22]. However, these theories have undetermined parameters, which inevitably leads to numerical or fitting methods. We must mention that they are insufficient because many related and actual physical parameters (i.e., physical constants) should be involved when the properties of high-T_c cuprates are considered.

For example, several researchers claim that, because of the existence of magnetic-field interactions, the natural force to combine a Cooper pair must be spin interactions. However, as will be mentioned in this study and our previous study [1], magnetic-field interactions are not generally only the spin interactions. Furthermore, the spin-fluctuation [22] model is a numerical one; in this sense, this model is similar to the Hubbard-like model [23].

These models have multiple parameters to determine or to fit; thus, they do not reflect actual physical picture the high-T_c cuprates originally have. Moreover, if the interaction was defined as spin interactions, they could not explain why other multiple physical parameters such as phonons are related [24,25].

That is, thus far research-related challenges have been prevented from a complete investigation of the abovementioned issues. If the calculations can be analytically solved, condensed matter physics will make considerable progress in developing then methods for fabricating compounds with higher critical temperatures could be developed through condensed matter physics fields. Thus, uncovering the physical mechanics of high-T_c cuprates is urgently required, and has motivated the present study. We thus provide new answers to the above questions.

Briefly, the understanding of high-T_c cuprates requires

1. Analytical calculations of many-body interactions. Most theories use a numerical or fitting method; however, these approaches cannot clarify the physical picture in high-T_c cuprates.
2. To understand the nature of the force to combine a Cooper pair over long distance.

Combining with our previous study [1], we will propose a concept of macroscopic Boson. This paper will describe the mechanism of high-T_c cuprates, using only this concept, with the consideration of many-body interactions. That is, basically, just only the existence of the macroscopic Boson will describe the mechanism of high-T_c cuprates.

As the contents of this paper, first we introduce a concept of macroscopic Boson, in which its mass and spin are described. Then using the partition function, the pseudo-gap energy is explained. Moreover, the method to handle many-body interaction will be introduced. Next, as the review of our previous article, we obtain the formula of T_c [1]. The calculations of obtaining formulas of T^* and T_0 are positioned, analyzing anomaly metal phases. Section 3 is Method in which more concrete

calculation methods are indicated. Then Result and Discussion sections are followed. Finally, the paper concludes the entire contents in section 6.

2. Theory

Let us consider a theoretical structure briefly. This theory is based on the emergence of a Macroscopic Boson under the transition temperature T_0. Moreover, the mass of this Boson is related to the pseudo-gap temperature T^*. Then for calculations of the critical temperature T_c, there are two ways in the derivation: the one comes from the combination of the macroscopic Bosons (i.e., Cooper pairs) and the other is originated from handling many-body interaction of the macroscopic Bosons. However, this paper will discuss that these two ways are essentially same. Afterwards, this paper will consider the anomaly metal phases based on the partition function of the Bosons. The common point is that every property in the cuprates is represented only by the assumption of the macroscopic Bosons.

Moreover, as a material, the present theory assumes that

i)   it has a CuO_2 2-dimensional surface, and

ii)   its carries are holes (i.e., electron carries are not handled in this paper).

2.1. Introduction of New Particle and Pseudo-Gap Relating to the New Particle

2.1.1. Introduction of a Macroscopic Boson

When considering a CuO_2 surface as the most important point [25] and when the refrigeration is sufficient such that a hole's wavelength becomes larger than that of width of the surface, it is assumed that 2D is completely formed. This indicates that, on the surface, an angular momentum must be conserved; thus, each hole takes a circle by self-rotating. At this time, because this rotating circle has magnetic field energy, we consider that a new particle has been created. Note that the creations of the particles imply a phase transition T_0, which will be described later in this paper. This is related to the electron nematic phase [26]. Going forward, we refer to this new particle as a "macroscopic Boson"; the schematic is shown in Figure 1.

For a literature support of the assumption of a macroscopic Boson, please refer to [27]. Moreover, this fact corresponds to the fact that, in a CuO_2 surface, a local persistent current exists [26].

$$T > T_0 \qquad\qquad\qquad\qquad T \leq T_0$$
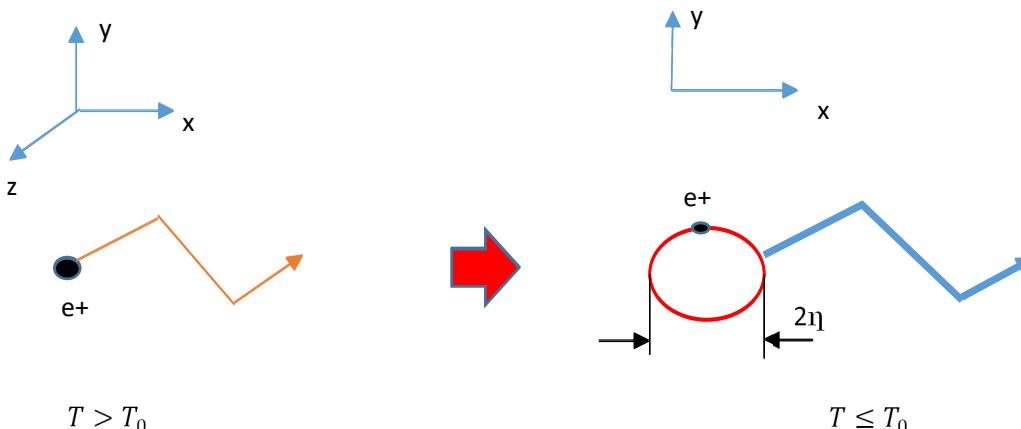
Figure 1. Schematic of a macroscopic Boson. Normally, holes move in 3D when their kinetic energy is high. However, when refrigeration reduces the momentum along z-direction, the complete x-y 2D motion is formed. Thus, a conservation of the angular momentum creates a rotation movement by a hole itself. This transition will be described later. Because a current circle by the rotation generates magnetic field energy, which determines the mass of this circle, this circle is essentially different from a normal hole. We will refer to this new particle as "a macroscopic Boson." The radius η of a macroscopic Boson is assumed to be of the order of a CuO_2 cell (i.e., ~1 nm).

2.1.2. Calculating the Mass of a Macroscopic Boson

First, let us calculate the mass of a macroscopic Boson. Generally, magnetic field energy is represented as follows:

$$2U = \frac{1}{2}I\Phi_0 - \overrightarrow{\mu_s} \cdot \vec{H} = \frac{1}{2}I\Phi_0 - \mu_{s,z}H_z \tag{1}$$

where I, Φ_0, $\overrightarrow{\mu_s}$ and $\vec{H}$ denote a current surrounding a macroscopic Boson, the magnetic flux of a macroscopic Boson having a unique value, the spin magnetic moment of a hole, and the generated magnetic field in the macroscopic Boson. Note that it is assumed that the magnetic field direction is along the z-axis. Moreover, if we do not substitute the more concrete equation of $\mu_{s,z}$, the second term is formed generally in terms of the electromagnetism. If we assumed that the particle is a fermion, then $\mu_{s,z}$ would have both the positive and the negative numbers. However, as will be mentioned later, at a temperature T_0, the identical and uniform particles are emerged. This implies that the uniformed energy U requires that $\mu_{s,z}$ be zero. Therefore, the particle must be a boson.

Considering the same reason, the flux must be quantized as

$$\Phi_0 = \frac{h}{e}, \tag{2}$$

where h and e denote the Planck constant and the charge of a hole, respectively. Note that this study used both the constants h and $\hbar$ as Planck constants.

In the current of Equation (1), the cyclotron angular frequency is introduced.

$$I = \frac{e}{T} = 2\pi e \omega_c = 2\pi e \frac{eB_0}{m} = 2\pi e^2 \frac{\mu_0 H_0}{m}, \tag{3}$$

where ω_c, B_0, and u_0 denote the cyclotron angular frequency, the constant and unique value of magnetic field in a macroscopic Boson, and the magnetic permeability in the vacuum, respectively. Thus, Equation (1) becomes

$$U = \frac{1}{2}2\pi e^2 \frac{\mu_0 H_0}{m}\frac{h}{e}, \tag{4}$$

where considering the flux of Equation (2)

$$H_0 = \frac{h}{e}\frac{1}{\mu_0 \pi \eta^2}, \tag{5}$$

where η is the approximated radius of a macroscopic Boson.

Because the magnetic field B_0 is expressed as Equation (5), the rest energy, i.e., the mass of a macroscopic Boson is formed as follows:

$$\mathbf{2U} = \boldsymbol{\pi}e^2 \frac{\boldsymbol{\mu_0}}{m}\frac{h}{e}\frac{1}{\mu_0 \pi \eta^2}\frac{h}{e} = \frac{h^2}{m\eta^2}. \tag{6}$$

2.1.3. Spin of a Macroscopic Boson

Let us now consider the spin of a macroscopic Boson. As mentioned, Equation (1) claims that the second term of this equation must be zero. This implies that the direction of spins of a hole and that of the magnetic field is perpendicular. Thus, if the direction of the magnetic field is assumed to be z-axis, then the directions of hole spins must be x-or y-axis.

Therefore, using the Pauli matrix, this case considers only the x- and y-components.

$$s_x = \frac{\hbar}{2}\begin{pmatrix} 0 & 1 \\ 1 & 0 \end{pmatrix}. \tag{7-1}$$

$$s_y = \frac{\hbar}{2}\begin{pmatrix} 0 & -i \\ i & 0 \end{pmatrix}, \tag{7-2}$$

where i denotes the imaginary unit.

In this study, a spin angular momentum is defined as the determinant from the Pauli matrix. Thus, each determinant is as follows:

$$\det s_x = -\frac{1}{2}\hbar, \tag{8-1}$$

$$\det s_y = \frac{1}{2}\hbar. \tag{8-2}$$

Therefore, a net spin angular momentum of a macroscopic Boson is calculated as follows:

$$\mathbf{s} \equiv \mathbf{det}s_x + \boldsymbol{det}s_y = \mathbf{0} \cdot \hbar. \tag{9}$$

Next, let us consider the orbital angular momentum *l*:

$$l_z = \eta^2 m_h \omega_c, \tag{10}$$

where

$$\omega_c \equiv \frac{eB}{m_h}, \qquad \text{and} \tag{11}$$

m_h is the mass of a hole, and η is the radius of a macroscopic Boson.

Thus,

$$l_z = \eta^2 eB. \tag{12}$$

The magnetic flux is provided as

$$\Phi_B = \frac{h}{e} = \pi\eta^2 B. \tag{13}$$

Accordingly,

$$l_z = 2\hbar. \tag{14}$$

To conclude, the net spin *j* is

$$\boldsymbol{j} = \mathbf{0} \cdot \hbar + \mathbf{2}\hbar = \mathbf{2}\hbar, \tag{15}$$

which implies the macroscopic Boson is a boson.

The above result indicates that, although a single hole behaves as a Fermion, this macroscopic Boson on 2 D behaves as a boson. Thus, the name of this particle is derived from this fact. As described, as long as considering 2D, the statistic property would alter.

2.1.4. Obtain the Partition Function of Macroscopic Bosons

Because a macroscopic Boson on 2D follows the Bose's partition function, we simply must consider the following:

$$f_r = \frac{1}{\exp\left(\frac{E_i - E_F}{k_B T}\right) - 1}, \tag{16}$$

where E_i, $|E_F|$, k_B, and T denote energy, a chemical potential (i.e., $E_F < 0$), the Boltzmann constant, and temperature, respectively. An important point is that the exponential function is approximated as a Maclaurin series,

$$\boldsymbol{f}_r \approx \frac{1}{\frac{E_i - E_F}{k_B T} + 1 - 1} = \frac{k_B T}{E_i - E_F}. \tag{17}$$

This abovementioned partition function is very important because all properties in the anomaly metal phase in CuO_2-based superconductors are described using this partition function. We will see how this equation describes properties of the anomaly metal phase later.

Moreover, this equation has another expression. Because we are now considering the chemical potential from Bosons and the general boson partition function, the following equation generally holds:

$$E_F = E + k_B T ln\left(\frac{N_A}{n_i}\right), \tag{18}$$

where the absolute value of the second term must dominate the value of the first term because the chemical potential is negative, and where N_A denotes accepter concentration. Moreover, $\frac{N_A}{2n_i}$ indicates a doping parameter in this study. The number 2 is attached because of the presence of spins. Therefore, because n_i indicates the concentration of lattices, $\frac{N_A}{n_i}$ of the function *ln* is less than the value of the number 1 as long as we consider the image in which holes are doped in a Mott insulator (That is, if the carrier is an electron, $\frac{N_A}{n_i}$ of the function *ln* is more than the value of the number 1 in the Mott insulator). Using the equation above, the partition function, Equation (17), is translated as follows:

$$f_r = -[\ln\left(\tfrac{N_A}{n_i}\right)]^{-1} \ . \tag{(17-2)}$$

2.1.5. Calculate the Pseudo-Gap Energy

Let us calculate the pseudo-gap energy, which is directly related to the mass of a macroscopic Boson. First, we define the carrier concentration of macroscopic Bosons considering a 2D energy state density.

$$D_2(E) = \frac{m}{\pi\hbar^2} \equiv p_0, \tag{19}$$

$$n = \frac{1}{d}\int D_2(E)f_r \, dE, \tag{20}$$

where $D_2(E)$, n, and d denote energy state density in 2D, particle concentration, and width of the 2D sheet, respectively. An important point to note is that the parameter d [m] is consistently substituted by the number 1; however, the reason of the appearances in certain equations clarify the meaning of these equations. The integral for concentration (20) is simply because the energy state density in 2D is constant as indicated in Equation (19) and because partition function f_r is represented by Equation (17-2). In the process of this calculation of Equation (20), an energy E_0 appears as follows:

$$E_0 = -\frac{d}{p_0} n_0 \times \ln(\tfrac{N_A}{n_i}), \tag{21}$$

This energy E_0 is assumed to be essentially equal to the pseudo-gap energy. Combined with the mass of a macroscopic Boson, this pseudo-gap energy is represented as follows:

$$E_0 = -U \times ln\left(\tfrac{N_A}{n_i}\right) = -\frac{1}{2}\frac{h^2}{m\eta^2}\ln\left(\tfrac{N_A}{n_i}\right). \tag{22-1}$$

The abovementioned pseudo-gap energy equation has a coefficient for doping function *ln*. This factor is identical to the zero-point energy:

$$\frac{1}{2}\hbar\omega = \frac{1}{2}\frac{h^2}{m\eta^2}. \tag{22-2}$$

The above equation implies that this derived energy E_0 merely indicates a potential. In general, however, an energy gap appears or disappears involving a photon's emission or absorption, which has a momentum. This fact indicates that, for a potential to become a general energy gap, the potential is given the product of the fine-structure constant α, which includes characteristic impedance Z_0 for electromagnetic waves. Typically, the fine-structure constant α is determined as follows:

$$\alpha = \frac{Z_0 e^2}{4\pi\hbar} = \frac{1}{137.0}. \tag{23}$$

In Equation (23), the impedance Z_0 works as the specific impedance to electromagnetic waves. Thus, the net pseudo-gap energy $|\Delta|_0$ is derived as follows, which will give the temperature of pseudo-gap T^* as discussed later.

$$|\Delta|_0 = -\frac{1}{2}\frac{h^2}{m\eta^2}\alpha \times \ln(\tfrac{N_A}{n_i}). \tag{24}$$

2.2. Superconductivity with Consideration of Many-Body Interactions

It is necessary to describe why macroscopic Bosons undertake Bose–Einstein (BE) condensation by forming a pair from two macroscopic Bosons, although they have been already general Bosons such as Cooper pairs. In the previously published paper [1], we reported a new attractive force to combine particles from local current in a CuO_2 cell [26]. This local current is equal to both rotational and self-current, which creates the mass of macroscopic Bosons; hence, the result of the previous paper agrees with the descriptions in the present paper. Therefore, in this section, based on the understanding that two macroscopic Bosons form a pair, we describe why BE condensation occurs considering many-body interactions between Bosons.

2.2.1. Description of the Model and the Principle to Many-Body Interaction

There are many-body interactions among the carriers in various materials. In particular, this fact is essential to high-T_c cuprates because the general band theory cannot be applied. The many-body interactions of carriers indicate there are many local temperatures T_i in the materials, where i is index for a location. In other words, only in a temperature T_i, thermal equilibrium can be assumed. Figure 2 shows our model for handling many-body interactions. In this figure, a radius a_i forms a sphere shell, which has differential number dN and local temperature T_i. Moreover, in the center, a macroscopic Boson is presented. The immediately outer particles out of dN yield a pressure to this sphere shell, which is equal to the kinetic energies of particles in dN (i.e., it is represented by a temperature T_i). However, the central macroscopic Boson provides force of expansion, which indicates electrostatic energy, i.e., Coulomb interactions. Moreover, this case adds magnetic interactions between macroscopic Bosons as an expansion force. Note that it is assumed that the number N is sufficiently large and thus we can consider the differential dN.
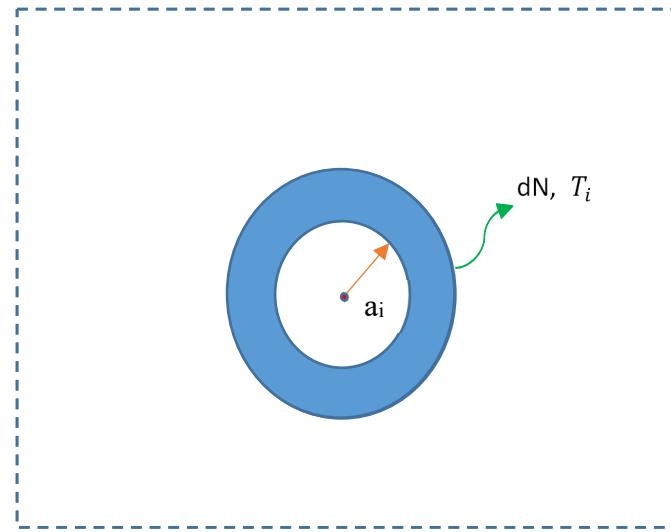
Figure 2. Schematic of our established model to handle many-body interactions. Considering the nature of many-body interactions, note that temperatures are locally different. However, this model claims that in the differential number dN (a macroscopic Boson takes the center and dN takes a temperature T_i), a thermal equilibrium can be assumed. Therefore, a balance between force of expansion from Coulomb interactions, in addition to the magnetic field interactions from the Bosons and force of compression from immediate outer side, which is equal to the kinetic energies in dN (i.e., a temperature T_i), is formed. Calculating this balanced equation results in a new statistical equation.

Considering that these forces of expansion should be balanced to a force of compression in a sphere shell, the following relation holds:

(Coulomb interaction energy and magnetic field interaction energy) $= \frac{3}{2} k_B T_i \times dN$

2.2.2. Calculate the Principal Equation of Our Model and the Internal Quantum State

Calculate the abovementioned principle-equation in the previous subsection. First, dN is represented as follows:

$$dN = \text{gfd}\vec{k} = gf(\frac{1}{dv}), \tag{25}$$

where k, v, g, and f denote wave number, volume, state number, and partition function for the Boson, respectively. In the equation of dN, as mentioned, state number g and partition function f are given as follows:

$$f \equiv f_r = -[\ln(\frac{N_A}{n_i})]^{-1}. \tag{17-2}$$

$$g = \frac{1}{d}\int D_2(E)dE = p_0 E_0, \tag{19-2}$$

$$D_2(E) = \frac{m}{\pi \text{h}^2} \equiv p_0, \tag{19}$$

$$E_0 = |\Delta|_0 = -\frac{1}{2}\frac{h^2}{m\eta^2}\alpha \times \ln(\frac{N_A}{n_i}). \tag{24}$$

Thus, fg is given as follows:

$$fg = p_0 \frac{1}{2}\frac{h^2}{m\eta^2}\alpha. \tag{26}$$

To calculate the left-hand side of the abovementioned balanced equation in principle of the previous subsection, the electrostatic energy U_E is calculated as follows:

$$U_E = \frac{1}{2}\varepsilon_0(\frac{e}{4\pi\varepsilon_0 a_i^2})^2 dv, \tag{27}$$

where ε_0 and a_i denote the permittivity for the vacuum and the radius which dN is taking in the model.

At this time, a volume element of the integral is expressed as follows:

$$dv = \frac{1}{d\vec{k}} = \frac{4\pi}{3}a_i^3. \tag{28}$$

Moreover, the magnetic interaction V_P from macroscopic Bosons is given as follows:

$$V_p = U_B dN. \tag{29}$$

Consequently, the resultant equation is provided by

$$a_i^2 = \frac{9\varepsilon_0}{e^2}(3k_B T_i - 2U_B)fg. \tag{30}$$

As shown in Figure 3, the central macroscopic Boson behaves under the model of the infinite well-potential. Thus, as every elementary quantum mechanics textbook [e.g.,[28]] describes, the eigenvalue and wave function of it are presented as follows:

$$\boldsymbol{\psi_i(r)} = \sqrt{\frac{2}{2a_i}}\sin(\frac{i\pi r}{2a_i}), \tag{31}$$

$$\boldsymbol{E_i} = \frac{1}{2M}(\frac{\hbar i\pi}{2a_i})^2, \tag{32}$$

where M, i, and r denote the mass of a macroscopic Boson, index, and microscopic variable of sphere-coordinates, respectively. These equations indicate that a particle under the many-body interactions forms a stationary wave and that the wave function of the stationary wave and the eigenvalue (i.e., kinetic energy) are determined by a radius a_i.
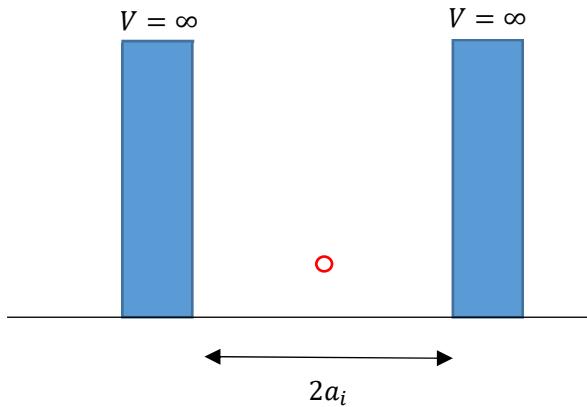
Figure 3. A basic model of infinite well-potential. This model is directly related to the immediate prior figure model. The diameter $2a_i$ varies depending on a temperature T_i. A macroscopic Boson in this well-potential forms a stationary wave, and its wave function and eigenvalue are presented in every basis textbook.

2.2.3. Describe BE Condensation and the Superconducting Transition

Using the abovementioned concept, we consider how BE condensation occurs. In addition to a sphere shell having temperature T_i, another sphere shell having temperature T_j is considered. When we accept a combination of two macroscopic Bosons by a force F, these two Bosons must have the identical kinetic energy because, in general and as mentioned in our previous paper [1], a relative and attractive force appears only when their relative velocities become the same. In particular, this fact is applied when an attractive Lorentz force is generated between moving and charged particles whose velocities are identical. Thus, when forming a pair from two macroscopic Bosons, the eigenvalues, Equation (32), indexed by i and j becomes equal. That is,

$$\left|E_i - E_j\right| = 0. \tag{33}$$

This indicates that an index i and j becomes equal, resulting in that all the radius a_i and eigenvalue E_i take the identical radius a_0 and E_B because of the arbitrary property of index i and j. Hence, if a pair forms, every energy of macroscopic Bosons undergoes the identical energy E_B, which indicates all the rest Bosons take pairs and BE condensation.

Moreover, as shown in Figure 4, considering index i to be equal j indicates that temperatures T_i and T_j must be equal. Even at this moment, positions r of wave functions, Equation (31), are common and thus the two sphere shells take the superposition, i.e., the relative distance ξ_G between the two sphere shells should be 0. Thus, the net coherence of two holes becomes on a cell order, 1 nm, as reported by many literatures. This physical picture is described as that one-unit cell has two-combined macroscopic Bosons and that, over the entire 2D surface, these unit cells having two macroscopic Bosons become uniform. Thus, by BE condensation, it can be assumed that the particle number is one and that $dN \rightarrow 0$. Therefore, the established shells vanish and thus the radius of $a_0 \rightarrow \eta$, which implies the rest interactions will be only for the neighboring particles, not many-body interactions.

As mentioned, the occurrence of BE condensation and forming two-combined Bosons are equivalent. Thus, a critical temperature can be obtained both by the way of the combination of the particles and by the approach of the many-body interactions.

Employing the abovementioned equation (30), an equation of the relative distance between sphere shells ξ_G for temperature T is derived as follows:

$$\frac{1}{4}\xi_G^2 = \frac{9\varepsilon_0}{e^2}(3k_B\langle T\rangle - 2U_B)gf, \tag{34}$$

where U_B is substituted with pseudo-gap $|\Delta|_0$ in Equation (24). Note that, in this equation, considering BE condensation and single-particle picture, p_0 of *gf* in Equation (26) is redefined as the value 1. As will be discussed in the Results section, temperatures at which $\xi_G^2 \leq 0$ indicates a superconductivity state and the transition temperature T_c at which $\xi_G = 0$ indicates a critical temperature.
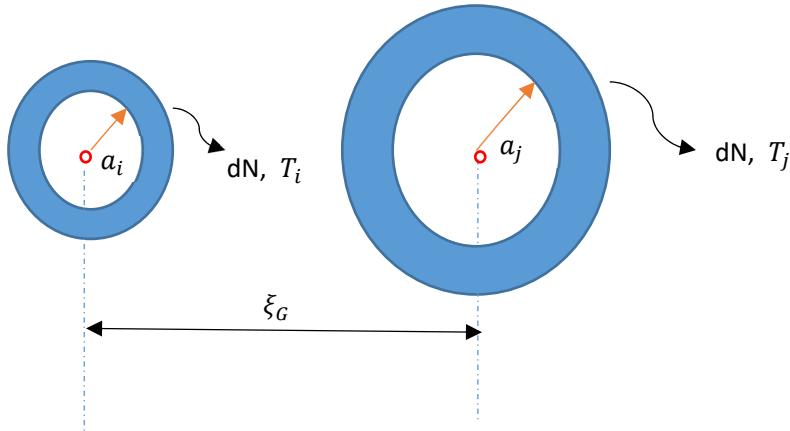
Figure 4. Schematic of two macroscopic Bosons having many-body interactions. The relative distance of $\boldsymbol{\xi_G}$ indicates one between two macroscopic Bosons. When an attractive force *F* between them appears and because the relative kinetic energy becomes 0, indexes *i* and *j* take the same. Thus, a superposition between them occurs, rendering $\boldsymbol{\xi_G}$ be 0. That is, two Bosons now combine to be a Cooper pair. Employing the statistic equations from our established model, we can predict this type of transition.

2.3. Review to Obtain the Formula for T_c

Note that this section is the review section for Ref. [1]

Herein, we would like to note the reason why there are Fermi energy and chemical potential E_F [29] in this paper. At this stage that two-macroscopic Bosons take a combination at a unit cell, although we cannot consider many-body interactions, there is a non-zero temperature, which is originated from the interaction for the neighboring Cooper pairs (i.e., $T \leq T_c$). This is equivalent to the fact that the neighboring holes in the Cooper pairs between unit cells collide with each other, which implies that each Cooper pair is repeatedly formed and destroyed [1]. Thus, only in the case of $T \leq T_c$, we consider the Fermi energy, i.e., $E_F \geq 0$.

2.3.1. Derivation of a General Energy Gap (Review)

Let us review our previous study [1], which describes a force *F* to combine two particles and a critical temperature T_c on doping. Note that because this is a review to understand the stream of outlined derivations of a critical temperature T_c, certain equations in the calculation and derivation processes are left out. In case that our readers are interested in the detail, the paper can be downloaded as an Open Access paper.

First, we assume that a general energy gap $|\Delta|$ is proportional to both Fermi energy and Critical temperature as follows [1]:

$$|\Delta|^2 = k_B T_c E_F. \tag{35}$$

In this equation, the Fermi energy in a p-type material [30] is employed as follows:

$$E_F = E_i - k_B T ln(\frac{N_A}{n_i}). \tag{36}$$

Note that we are considering the carrier is a hole.

In this equation, a superconducting energy gap is introduced.

$$2E_i = k_B T_c \tag{37}$$

Substituting these energies and employing the state equation with the universal gas constant *R*, the following equations are obtained.

$$|\Delta|^2 = \frac{1}{2}(k_B T_c)^2 \left\{ 1 - 2\frac{T}{T_c}\ln\left(\frac{N_A}{n_i}\right) \right\} \tag{38}$$

and

$$|\boldsymbol{\Delta}|^2 = \frac{1}{2}(\boldsymbol{k_B T_c})^2 \left\{ \mathbf{1} - \mathbf{2}\frac{1}{T_c}\frac{|\Omega_B|}{R}\frac{1}{\rho_s}\ln\left(\frac{N_A}{n_i}\right) \right\} \tag{39}$$

where

$$|\Omega_B| = pV. \tag{40}$$

where Ω_B denotes a thermodynamic potential, and ρ_s is the concentration of Cooper pairs. In this manner, a general expression of energy gap for temperatures was derived. Note that interactions between Cooper pairs and Cooper pairs is assumed to be relatively small (i.e., that is merely local and neighboring collisions), which justifies the employment of the state equation.

2.3.2. Generation of an Attractive Force that Combines Two Carriers (Review)

To consider the superconducting energy gap, it is necessary to mention a force *F*, which results in a combination of a Cooper pair. As previously mentioned, two charged particles generally experience an attractive force with each other when they are moving with the same velocity, i.e., when the relative energy or momentum is 0. As shown in Figure 5a–d, two parallel conductors along which the same direction and same amount of a current are presented. From the electromagnetism, these current leads experience an attractive force with each other, which is attributed to the Lorentz force. When we shorten these leads to a wavelength of a carrier, this attractive force still exists. This indicates that **two charged particles with identical wave numbers are attracted to each other. This attractive force stems from the Lorentz force.**

2.3.3. Derivation of T_c (Review)

Considering the principle of generating an attractive force and assuming that the wave function of a hole is a plane wave and that the magnetic field generated by the moving holes is derived from a linear current, the Lorentz force *F* is given as follows:

$$F = q^2 \frac{\hbar\mu_0}{m^2}\frac{4\pi^2}{k^2}\beta|\psi|^2 k^2 \frac{1}{2r}sin\theta cos\varphi = \frac{2q^2\pi^2\mu_0\hbar}{m^2}\beta|\psi|^2\frac{1}{r}sin\theta cos\varphi, \tag{41}$$

where ψ, r, θ, ϕ, q, β, k m, and μ_0 denote wave function of a hole, relative distance of two holes, angle associated with the Lorentz force, angle related with two wave number of holes, the electric charge of a hole, constant, common wave number, the mass of an electron, and magnetic permeability of the vacuum, respectively. Note that this equation employs the probability density flux as current density.

The energy *u* (i.e., superconducting energy gap) from the line integral of the above force *F* is represented as follows:

$$u = -\frac{2q^2\pi^2\mu_0\hbar}{m^2}\beta|\psi|^2\ln(r) \times sin\theta cos\varphi + u_0 \quad u_0 \leq 0, \tag{42}$$

where u_0 denotes an integral constant.

$$\alpha \equiv -\frac{2q^2\pi^2\mu_0\hbar}{m^2}\ln(\xi) \times sin\theta cos\varphi, \tag{43}$$

where ξ denotes the coherence of a Cooper pair.

$$u = \alpha\beta|\Psi|^2 + u_0. \tag{44}$$

It is assumed that $|\Delta|$ is proportional to T_c. That is, $|\Delta|$ is proportional to the energy *u*.

$$\alpha'|\Delta| = u = \frac{1}{2} k_B T_c \ , \tag{45}$$

$$\alpha'|\Delta| = \alpha\beta|\Psi|^2 + u_0. \tag{46}$$

Therefore, the relationship between α and α' is a linear dependence
That is,

$$\alpha' \equiv \rho\alpha. \tag{47}$$

According to the analysis of the dimension, the constant ρ has the unit [1/J].
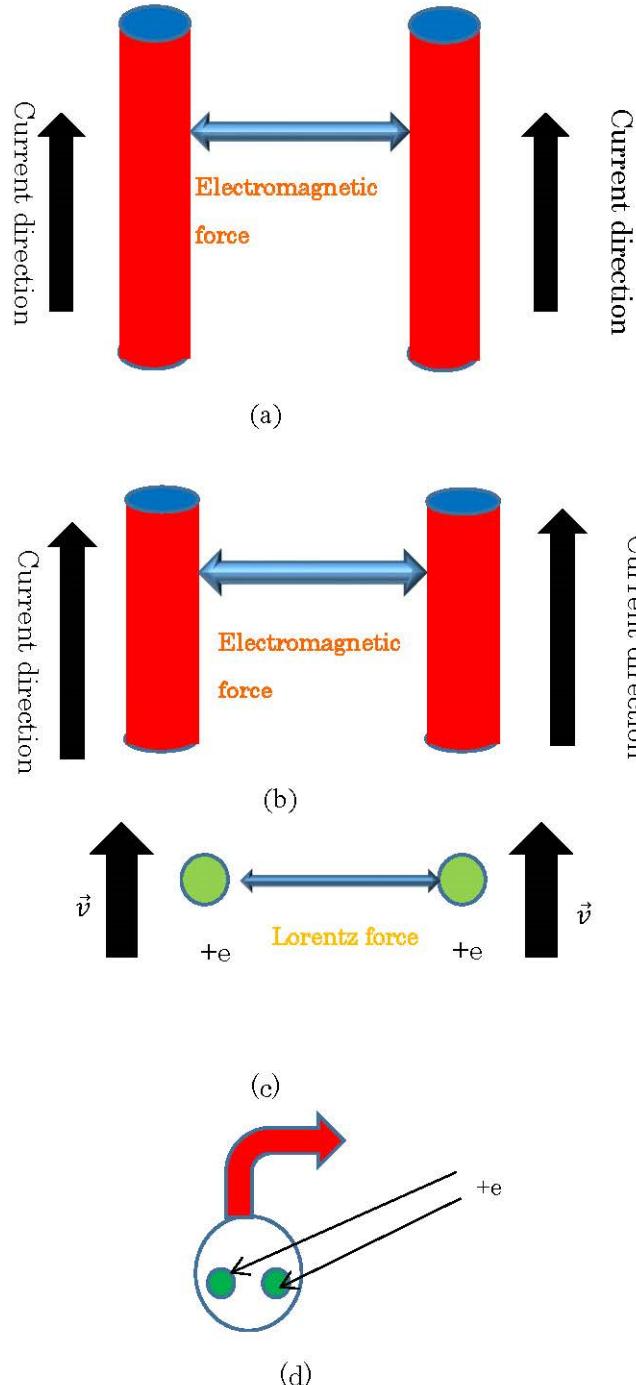
Figure 5. (a) Currents in the same direction. (b) Shorter leads with currents in the same direction. (c) Holes with same direction and equal velocity. (d) Center-of-mass motion of Cooper pair.

Thus, we can give the equation that

$$\rho \equiv \frac{1}{k_B \theta_D},$$
(48)

where k_B and θ_D denote the Boltzmann constant and the Debye temperature, respectively.

Equation (45) is squared:

$$\alpha'^2 |\Delta|^2 = \frac{1}{4} k_B^2 T_c^2.$$
(49)

That is,

$$|\Delta|^2 = \frac{k_B^2 T_c^2}{4\alpha'^2}.$$
(50)

From Equation (39),

$$\frac{k_B^2 T_c^2}{4\alpha'^2} = (k_B T_c)^2 \{\frac{1}{2} - \frac{1}{T_c} \frac{|\Omega_B|}{R} \frac{1}{\rho_s} \ln\left(\frac{N_A}{n_i}\right)\}.$$
(51)

By the organization of the above equation and the substitution of α',

$$T_c = -4[\frac{1}{k_B \theta_D}(-\frac{2q^2 \pi^2 \mu_0 \hbar}{m^2} \ln(\xi) \times \sin\theta\cos\varphi)]^2 \frac{|\Omega_B|}{R} \frac{1}{\rho_s} \ln\left(\frac{N_A}{n_i}\right).$$
(52)

In this equation, the thermodynamics potential is replaced by that of zero temperature, $|\Omega_B|_0$, and the integral constant $T_{c,m}$ is instead introduced. This implies that when $|\Omega_B| \to |\Omega_B|_0$, the difference is renormalized to $T_{c,m}$:

$$T_c = -4[\frac{1}{k_B \theta_D}(-\frac{2q^2 \pi^2 \mu_0 \hbar}{m^2} \ln(\xi) \times \sin\theta\cos\varphi)]^2 \frac{|\Omega_B|_0}{R} \frac{1}{\rho_s} \ln\left(\frac{N_A}{n_i}\right) - T_{c,m}.$$
(53)

where

$$T_{c,m} \equiv \theta_D \ [1]$$
(54)

and

$$|\Omega_B|_0 = p_0 V,$$
(55)

where p_0 and V denote the pressure and volume, respectively.

Again,

$$T_c = -4\alpha'^2 \frac{|\Omega_B|_0}{R\rho_s} \ln\left(\frac{N_A}{n_i}\right) - \theta_D \ ,$$
(56-1)

where

$$\alpha = -\frac{2q^2 \pi^2 \mu_0 \hbar}{m^2} \ln(\xi) \times \sin\theta\cos\varphi \ ,$$
(56-2)

$$\alpha' = \frac{1}{k_B \theta_D}\alpha = -\frac{1}{k_B \theta_D}\frac{2q^2 \pi^2 \mu_0 \hbar}{m^2} \ln(\xi) \times \sin\theta\cos\varphi \ .$$
(56-3)

In this process, we added a Debye temperature θ_D and a net coherence ξ to the equations. Note that, to an integral constant $T_{c,m}$ in Equation (53), the BCS formula under a particular condition was employed. That is, in the formula T_c of the BCS theory, because the Boson combination energy in high-T_c cuprates is generally sufficiently large, which attributed to the short coherence (note that, the shorter the coherence is, the larger the magnetic field associated with the Lorentz force becomes), the large value of NV in the BCS formula of T_c makes the exponential function be almost the value 1. Thus, only the Debye temperature in the BCS formula is left. Concerning the thermodynamic potential, the following equation is applied under the condition of BE condensation.

$$|\Omega_B|_0 = p_0 V = \frac{2}{5} E_{F0},$$
(57)

where E_{F0} denotes the Fermi energy at zero temperature. Moreover, here the volume V is assumed to be the unit, i.e., the number 1. Thus, the critical temperature becomes

$$T_c = -4 \left(\frac{1}{k_B\theta_D}\right)^2 (\frac{2q^2\pi^2\mu_0\hbar}{m^2}\ln(\xi) \times sin\theta cos\varphi)^2 \frac{2F_{F0}}{5R\rho_s}\ln\left(\frac{N_A}{n_i}\right) - \theta_D \ . \tag{58}$$

Moreover, we derive a 2D critical temperature equation from the above. Thus, to conclude, the critical temperature equation is derived as follows:

$$\langle T_c\rangle_2 = -4 \left(\frac{1}{k_B\theta_{D2}}\right)^2 (\frac{2q^2\pi^2\mu_0\hbar}{m^2}\ln(\xi) \times sin\theta cos\varphi)^2 \frac{2F_{F0}n_q}{5R\sigma_s}\ln\left(\frac{\sigma}{n_{i2}}\right) - \theta_{D2} \tag{59}$$

where σ, σ_s, θ_{D2}, and n_q denote the surface density of carriers, the surface density of pairs, Debye temperature in 2D, and the number of layers. Note that all constants in the consequent equation have actual physical meaning and unit. This indicates that no numerical calculations or fitting methods are required. This fact is consistent everywhere in the present study.

Note that, in Equation (42) for the superconducting energy gap, the probability density function is interpreted as follows:

$$|\psi|^2 sin\theta cos\varphi = |\psi|^2 sin\theta \sin\left(\varphi + \frac{\pi}{2}\right) = \frac{1}{2}|\psi|^2\left\{-\cos\left(\theta + \varphi + \frac{\pi}{2}\right) + \cos\left(\theta - \varphi + \frac{\pi}{2}\right)\right\} \tag{60}$$

which shows that the gap is anisotropic [31].

Note that we assume that θ_{D2} and E_{F0} are not varied very much over kinds of the cuprates. In Figure 6, a result of this review section is shown where used physical parameters are listed in Table 1. Note that for additional details, please see the Method section at which the full list of employed physical constants are presented. As shown, our derived critical temperature equation sufficiently agrees with a typical high-T$_c$ copulate [32]. Note that the reason why the Fermi energy is relatively large is related to the property of the Mott insulator. For more details, please refer to [1].
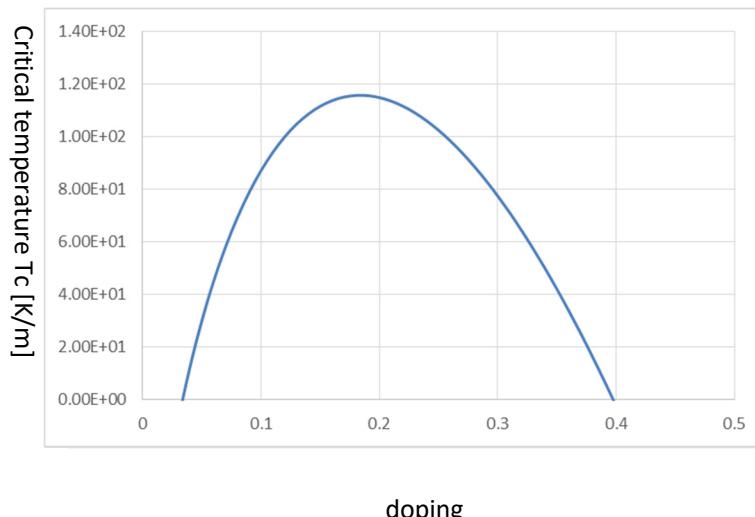
Figure 6. A result of typical critical temperature on doping. This is derived from the equation by combining pseudo-gap energy (i.e., the general energy gap) and superconducting energy gap. At doping 0.16, the critical temperature reaches the maximum, which agrees with the experiments [e.g., [32]] In calculations, no numerical calculations or fitting method are employed. The values of critical temperatures are relatively sensitive for Debye temperature and Fermi energy in our derived equation.

Table 1. Physical parameters in the equation of critical temperature.

Debye temperature θ_{D2}	113.5 K
Coherence ξ	1 nm
Fermi energy E_{F0}	7.65×10^{-19}J
The number of layer n_q	3

2.4. Calculations for Obtaining Formulas for T and T₀*

2.4.1. Derive the Pseudo-Gap Temperature T*.

Now, we again consider the relation between a general energy gap and temperature, as shown in Equation (38)

$$T = -\frac{|\Delta|^2}{k_B^2}\frac{1}{T_c}\frac{1}{\ln\left(\frac{N_A}{n_i}\right)},$$ (38)

When the previously derived energy gap from a macroscopic Boson is substituted for an energy gap in the abovementioned equation, then variable temperature *T* must become a constant of pseudo-gap temperature *T**. Therefore, the temperatures *T*c and *T** have a dependent relationship. Thus, as a formula of pseudo-gap temperature *T**, the following equation holds:

$$\boldsymbol{T^*} = -\frac{1}{k_B^2}\frac{1}{4}(\boldsymbol{3.4\times10^{-21}})^2\left[\ln\left(\frac{N_A}{n_i}\right)\right\}^2\frac{1}{T_c\ln\left(\frac{N_A}{n_i}\right)} = -\frac{1}{k_B^2}\frac{1}{4}(\boldsymbol{3.4\times10^{-21}})^2\left[\ln\left(\frac{N_A}{n_i}\right)\right\}^{\square}\frac{1}{T_c},$$ (61)

where to the equation of $|\Delta|_0$ of Equation (24) in creating Equation (61), each physical parameter was substituted. That is, the physical parameters *m*, *h*, and *α* in Equation (24) were given actual values. Note that radius *η* is approximated as 1 nm.

2.4.2. Derive the Transition Temperature T₀

In this study, we consider the anomaly metal phase properties in CuO_2–based superconductors. These properties are primarily determined by the transition temperature *T₀*, which is directly related to appearances of the macroscopic Boson as particles. To obtain an equation for the temperature *T₀*, we consider first the concentration dependent on the magnetic fields. Next, derivations of the Hall-effect coefficient RH are discussed. The concentration depends on absolute of energy, –uBe, where *u* and *B*e denote self-magnetic moment of a macroscopic Boson and applied magnetic field, respectively. That is, the absolute of energy, uBe, involves Boltzmann statistics and thus it is related to concentration (i.e., the number) of macroscopic Bosons.

In the previously appeared concentration Equation (20), the calculation for energy integral, in turn, is actually conducted because we attempted to obtain the concentration dependent on temperature *T*.

$$n = k_B T\frac{1}{d}p_0\int_a^b\frac{dE}{E-E_F} = k_B T\frac{1}{d}p_0\times\ln\left(\frac{T_0}{T_c}\right),$$ (62)

where

$$a = k_B T_c \qquad b = k_B T_0$$ (62-2)

Note that the second form of *fr* in Equation (17-2) is not employed here. Equation (62) is very important because the concentration *n* is proportional to the temperature *T*, which describes a property of the anomaly metal state. As mentioned, considering an energy –uBe, the Boltzmann statics is represented as follows:

$$n = n_0\exp\left(-\frac{\mu B_e}{k_B T}\right),$$ (63)

where *n₀* is the concentration of holes and *n* implies that the concentration of the macroscopic Bosons whose orbital momenta are the same directions as that of the magnetic field *B*e.

$$\boldsymbol{T_0} \equiv \frac{\mu B_e}{k_B}$$ (64)

Using the above equation,

$$n = n_0\exp\left(-\frac{T_0}{T}\right) \approx n_0\left[1-\frac{T_0}{T}\right]$$ (63-2)

Note that, in the above equation, $\frac{T_0}{T} \leq 1$ is formed as the condition, because the concentrations n and n_0 must be positive. When $T \to \infty$, the number of holes is equal to that of the macroscopic Bosons, which implies that the net number of the macroscopic Bosons takes zero. This is equivalent to zero magnetic fields when considering Equation (63). However, after the refrigeration, in the boundary condition, $\frac{T_0}{T} \equiv 1$, obviously a transition temperature is defined, which implies the emergence of a macroscopic Boson.

Now we begin to calculate RH.

In Equation (63), the exponential function is approximated by the Maclaurin series.

$$n \approx n_0(1 - \frac{\mu B_e}{k_B T}). \tag{65}$$

In the above equation, the previously calculated concentration n, Equation (62), is applied.

$$k_B T \frac{p_0}{d} \times \ln(\frac{T_0}{T_c}) = n_0(1 - \frac{\mu B_e}{k_B T}). \tag{66}$$

Solving this equation for n_0 and using the general definition of RH, we reach an important equation.

$$R_H = \frac{\frac{\mu B_e}{k_B T} - 1}{e k_B T \frac{p_0}{d} \times \ln(\frac{T_0}{T_c})}. \tag{67}$$

Considering the above equation (67), we also derive the transition temperature T_0, Equation (64). In short, the transition temperature T_0 implies appearances of both a macroscopic Boson and anomaly metal phase

2.4.3. Implement the Formulation of T_0

To implement the formula T_0, it is necessary to obtain u and B_e in Equation (64). First, a magnetic moment u is generally defined as follows:

$$\mu = IS, \tag{68}$$

where I and S ($\approx \eta^2$) denote the self-current and the area in which a magnetic flux is presented. Seeing the schematic of Figure 1 of a macroscopic Boson (which assumes the motion of a hole to be a circle) and because the magnetic flux of it should be quantized as h/e, the magnetic flux of a macroscopic Boson is as follows:

$$\Phi_0 = B_0 \pi \eta^2 \equiv \frac{h}{e}. \tag{69}$$

That is,

$$B_0 = \frac{h}{e} \frac{1}{\pi \eta^2}, \tag{69-2}$$

where radius η is approximated on a cell of the CuO$_2$ surface. That is,

$$\eta \approx 1 \text{ nm} \tag{70}$$

This implies that the magnetic field B_0 is universally constant.

Moreover, assuming that a magnetic field in a macroscopic Boson is equal to the central magnetic field generated by a moving hole, a persistent current I in a magnetic moment is calculated as follows:

$$I = \frac{1}{\mu_0} 2\eta B_0. \tag{71}$$

Consequently, a magnetic moment u is derived as follows:

$$\boldsymbol{\mu \approx \frac{2}{\mu_0} \eta \frac{h}{e}}. \tag{72}$$

While an applied magnetic field B_e in the definition of T_0 is variable, the magnetic field B_0 is a constant derived by the physical constants. This fact allows us to introduce a variable quantum number N between B_e and B_0

$$B_0 \frac{1}{N} = B_e. \tag{73}$$

Moreover, this variable integer N is undergone by the partition function *fr*.

$$N = N_0 f_r, \tag{74}$$

where Equation (17-2) is applied as *fr*.

However, without an external applied magnetic field, high-T_c cuprates generally achieve superconductivity. Why do our high-T_c cuprates become superconductive by forming many independent macroscopic Bosons? This can be understood by considering an analogy that every magnetic moment in a ferromagnetic material spontaneously acquires the same orientation under Curie temperatures. Thus, high-T_c cuprates have a property that is similar to a ferromagnetic material. We claim that this fact is related to the electronic nematic phase [26].

In this case, because macroscopic Bosons are formed in 2D CuO_2 surface, the weak interactions between macroscopic Bosons can justify the abovementioned calculation. The appearance of temperature T in Equation (63) guarantees the existence of these weak interactions. (The actual calculations of Curie temperatures with complete consideration of many-body interactions are presented in the Appendix A of this study.)

Assembling these facts, the conclusive equation of the transition temperature T_0 is derived, which depends on carrier doping.

$$\boldsymbol{T_0} \approx -\frac{1}{k_B} \left(\frac{2}{\mu_0} \boldsymbol{\eta} \frac{h}{e}\right) \left(\frac{h}{e\pi\eta^2}\right) \frac{1}{N_0} \ln\left(\frac{N_A}{n_i}\right). \tag{75}$$

As described later, this equation of T_0 and the formula of critical temperature T_c will be crucial factors when calculating properties of the anomaly metal phase.

2.5. Analyze Anomaly Metal Phase

2.5.1. More Comprehensive Calculation of RH

Next, we derive dependences on temperature of RH. Up to the previous section, the general equation of RH was derived. In this equation, we introduce the following approximation to the general equation of RH.

$$\frac{\mu B_e}{k_B T} \gg 1. \tag{76}$$

According to this approximation, the general equation of RH becomes as follows:

$$R_H \approx \frac{\mu B_e}{e(k_B T)^2 \frac{p_0}{d} \times \ln\left(\frac{T_0}{T_c}\right)}. \tag{77}$$

Thus, the approximated equation of RH is determined by the applied magnetic fields B_e. That is, this RH equation depends on both quantum number N and the universal magnetic field B_0.

$$R_H \approx \frac{\mu B_0}{e(k_B T)^2 \frac{p_0}{d} \times \ln\left(\frac{T_0}{T_c}\right)} \frac{1}{N}. \tag{78}$$

Note that the universal magnetic field B_0 is one in a macroscopic Boson. Thus, in view of magnetic field energy, an application of magnetic field, which dominates over the universal magnetic field B_0 results in the destructions of macroscopic Bosons and makes the anomaly metal phase disappear. Moreover, the employment of quantum number N indicates that the RH equation is determined by doping. That is, variable integer N is expressed by the partition function *fr*, which indicates doping.

$$\frac{1}{N} = \frac{1}{N_0 f_r} = -\frac{1}{N_0} \times \ln\left(\frac{N_A}{n_i}\right). \tag{79}$$

Considering this, the approximated RH equation becomes

$$\boldsymbol{R_H} \approx -\frac{\mu B_0}{e(k_B T)^2 \frac{p_0}{d} \times \ln\left(\frac{T_0}{T_c}\right)} \frac{1}{N_0} \times \ln\left(\frac{N_A}{n_i}\right). \tag{80}$$

As reported in many studies [33], this derived equation of RH is proportional to $\left(\frac{1}{T}\right)^2$.

In the Results section, we will depict this RH equation in terms of both doping parameters and temperatures T.

2.5.2. Calculate the Electron Specific Heat Coefficient in the Anomaly Metal Phase

In turn, let us consider electron specific heat coefficient in the anomaly metal phase. Because electron specific heat coefficient is essentially equal to the average energy U_E, it is simply necessary to calculate the average energy using the partition function fr. Thus, average energy using partition function fr (Equation (17)) for energy integrals is determined as follows:

$$U_E = \frac{\int E f_r dE}{\int f_r dE}. \tag{81}$$

Note that the lower limitation a and the upper limitation b of these integrals are given as follows:

$$\mathrm{a} = k_B T_c \quad b = k_B T_0. \tag{82}$$

Assuming the chemical energy for macroscopic Bosons (i.e., not Fermi energy for single holes) is sufficiently small, the calculation results in

$$U_E = \frac{k_B T_0 - k_B T_c + E_F \times \ln(\frac{k_B T_0 - E_F}{k_B T_c - E_F})}{\ln(\frac{k_B T_0 - E_F}{k_B T_c - E_F})} \approx \frac{k_B (T_0 - T_C)}{\ln(\frac{T_0}{T_c})}. \tag{83}$$

In general, electron specific heat coefficient is derived by differential in terms of temperature to the average energy. In this study, however, ΔT is employed rather than the differential for temperature. Moreover, this ΔT is assumed to be $(T_0\text{-}T_c)$ in this study. Therefore, using the average energy U_E and ΔT, electron specific heat coefficient is expressed as a calculation process.

$$\gamma_0 = \frac{U_E}{(\Delta T)^2} = \frac{k_B}{T_0 - T_c} \frac{1}{\ln(\frac{T_0}{T_c})}. \tag{84}$$

Furthermore, to obtain electron specific heat coefficient with the unit [J/mol K²], the Avogadro constant N_0^A is considered because previously calculated average energy U_E indicates one for a macroscopic Boson. Consequently, the electron specific heat coefficient is derived as follows:

$$\gamma = \frac{N_0^A k_B}{T_0 - T_c} \frac{1}{\ln(\frac{T_0}{T_c})}. \tag{85}$$

2.6. Summary of the Logical Flow

(1) First, assuming a macroscopic Boson, which is based on angular momentum conservation on a CuO_2 surface, its energy, the mass, and the net spin were calculated; the implementation of the integral of the concentration resulted in a pseudo-gap energy. During this process, the two types of partition equations fr were derived.

(2) To handle many-body interactions, a sphere shell with a local temperature T_i and differential particle number dN is introduced. From the forces that are balanced for both inside and outside the shell, a basic statistic equation, inner wave function and eigenvalue in a shell were derived.

(3) The generation principle of attractive force: "The Lorentz force is applied between two charged particles when their relative velocity is 0." Considering this principle, the abovementioned statistic equation, inner wave function and inner eigenvalue realize that the combination of a Cooper pair results in BE condensation.

(4) Therefore, the superconducting energy gap and T_c were calculated. During this process, a general energy gap is derived.

(5) Combining the general energy gap and the mass of a macroscopic Boson, the pseudo-gap temperature, T^*, formula was obtained.

(6) The transition temperature T_0 at which anomaly metal phase and the macroscopic Bosons appear was defined by the Boltzmann statistics: Combining the Boltzmann statistics, particle concentration was implemented. Considering the form of this equation, the transition temperature T_0 was derived.

(7) Because the resulted T_0 has the magnetic moment of a macroscopic Boson u and magnetic field

B_e, these two factors were formulated. Thus, the T_0 formula was implemented.

(8)   The derived RH equation was approximated, and electron specific heat coefficient γ was calculated.

3. Methods

Herein, we describe the detailed method for the Results section.

3.1. Calculation Tool

We employed the MS Excel software.

3.2. Physical Constants for Calculations

Table 2 shows the primary physical constants in this study. Of note, although Debye temperatures for 3D and 2D are different, we employed 2D one

Table 2. Physical constants in the obtained equations.

Debye temperature θ_{D2}	113.5 K
Coherence ξ	1 nm
Fermi energy E_{F0}	7.65×10^{-19}J
The number of layer n_q	3
Boltzmann constant k_B	1.38×10^{-23}J/K
Magnetic permeability in vacuum μ_0	$4\pi \times 10^{-7}$H/m
Electron mass m	9.1×10^{-31}kg
Electric charge of an electron e or q	$1.6 \times 10^{-19}C$
Radius of a macroscopic Boson η	1×10^{-9}m
Planck constant 1 h	$6.62 \times 10^{-34}J \cdot s$
Planck constant 2 $\hbar$	$1.05 \times 10^{-34}J \cdot s$
Fine structure constant α	1/137
Avogadro constant N_A^0	$6.0 \times 10^{23} \ mol^{-1}$
Permittivity in vacuum ε_0	$8.8 \times 10^{-12}F/m$
Universal gas constant R	8.31 $J \cdot mol^{-1} \cdot K^{-1}$

3.3. Resulted Equations

3.3.1. Critical Temperature

$$\langle T_c \rangle_2 = -4\left(\frac{1}{k_B\theta_{D2}}\right)^2 \left(\frac{2q^2\pi^2\mu_0\hbar}{m^2}\ln(\xi) \times sin\theta cos\varphi\right)^2 \frac{2E_{F0}n_q}{5R\sigma_s}\ln\left(\frac{\sigma}{n_{i2}}\right) - \theta_{D2} \ . \tag{59}$$

The critical temperature is shown above again. Concerning anisotropic properties, sine and cosine are given the maximum values of 1. Table 2 lists the physical constants used except for concentrations.

3.3.2. How to Determine n_i and ϱ_s

In Equation (59), $\frac{\sigma}{n_{i2}}$ is identical for $\frac{N_A}{n_i}$, because the length along the c-axis, d, is consistently given the value of 1 by considering the 2D surface. Moreover, it is necessary to determine the values of $1/\sigma_s$, i.e., $1/\varrho_s$ when given the doping variable $\frac{N_A}{2n_i}$ as follows:

(How to determine n_i)

In this study, the concentration n_i indicates lattice concentration. Because the unit cell of the CuO_2 surface is of the 1-nm order, the following assumption is introduced

$$2n_i = \frac{1}{d}\frac{1}{(10^{-9})^2} = \frac{1}{d} \times 10^{18}, \quad [1/m^3] \tag{86}$$

Note that d has the unit of [m] and the consistent value of 1 because we are considering two dimensions.

Because the critical temperature Equation (59) uses the universal gas constant,

$$R = 8.31 \ [J \cdot mol^{-1} \cdot K^{-1}], \tag{87}$$

the concentration n_i must be transformed into one with the unit [mol/L].

Thus, consider the following:

1) Avogadro constant N_A^0

2) $1[L] = 10^{-3} \ [m^3]$

Therefore, the concentration n_i is typically

$$n_i = \frac{1}{d} 8.3 \times 10^{-10} [\text{mol/L}]. \tag{88}$$

(How to determine $1/\rho_s$)

First, in the MS Excel sheet, the variable-doping ratio $\frac{N_A}{2n_i}$ is in the range of 0.005–0.5. Note that the number 2 appears due to spins. Then, $\frac{N_A}{n_i}$ is calculated based on the abovementioned variable doping ratio.

$1/\rho_s$ should be determined by the constant concentration, Equation (88)

$$\frac{1}{\rho_s} = x \frac{1}{n_i} \ , \tag{89-1}$$

where x denotes dimensionless variable. To give Equation (89-1) the meaning, variable x is provided as

$$x = \frac{N_A}{n_i}. \tag{89-2}$$

3.3.3. Pseudo-Gap Temperature and Transition Temperature at which an Anomaly Metal Phase Occurs

We list the results of each transition temperatures, which will be shown in the Results section.

$$\boldsymbol{T^*} = -\frac{1}{k_B^2}\frac{1}{4}(\boldsymbol{3.4 \times 10^{-21}})^2 [\ln(\frac{N_A}{n_i})\}^{\square} \frac{1}{T_c}. \tag{61}$$

$$\boldsymbol{T_0} \approx -\frac{1}{k_B}(\frac{2}{\mu_0}\boldsymbol{\eta}\frac{h}{e})(\frac{h}{e\pi\eta^2})\frac{1}{N_0}\ln(\frac{N_A}{n_i}). \tag{75}$$

Of note, $N_0 \approx 1.0 \times 10^6$, for example.

3.3.4. Physical Results of the Anomalous Metal Phase

(Hall effect coefficient)

$$\boldsymbol{R_H} \approx -\frac{\mu B_0}{e(k_B T)^2 \frac{p_0}{d} \times \ln\left(\frac{T_0}{T_c}\right)}\frac{1}{N_0} \times \ln(\frac{N_A}{n_i}). \tag{80}$$

Of note, $N_0 = 1.1 \times 10^2$, for example. Because B_0 is constant, the variation of integer N_0 indicates variation in the applied magnetic field B_e,

Moreover, in the abovementioned resulting equation, the following constants were employed.

$$\mu \approx \frac{2}{\mu_0}\eta\frac{h}{e}, \tag{72}$$

$$B_0 = \frac{h}{e}\frac{1}{\pi\eta^2}, \tag{69-2}$$

$$\frac{m}{\pi h^2} \equiv p_0, \tag{19}$$

(Electron specific heat coefficient)

$$\gamma = \frac{N_0^A k_B}{T_0 - T_c} \frac{1}{\ln(\frac{T_0}{T_c})}.$$ (85)

3.3.5. Results of the Many-Body Interaction Model

$$\frac{1}{4}\xi_G^2 = \frac{9\varepsilon_0}{e^2}(3k_B\langle T\rangle - 2U_B)\boldsymbol{gf},$$ (34)

where

$$gf \equiv p_0 \frac{1}{2}\frac{h^2}{m\eta^2}\alpha.$$ (26)

Of note, in Equation (26), considering the BE condensation and single-particle picture, $p_0 \equiv 1$

$$U_B = E_0 = |\Delta|_0 = -\frac{1}{2}\frac{h^2}{m\eta^2}\alpha \times \ln(\frac{N_A}{n_i}).$$ (24)

The doping variable is fixed as a constant only in the abovementioned equation.

$$\frac{N_A}{2n_i} \equiv 0.16 \ (optimal).$$

3. Results

As a general notation, for the comparisons between the experiments and the values of our theory, this paper cited the experimental literatures in each case. Overall, the agreements are good.

First, Figure 7 shows the entire depictions of T_c, T^*, and T_0 on doping because of analytical calculations. Generally, the agreements with the experiments are good [e.g., 32]. Moreover, in Figure 8, the result of theoretical calculations of the Hall coefficient RH is indicated. As shown, the lower doping, the higher RH, and the RH behave as non-linear on temperatures.
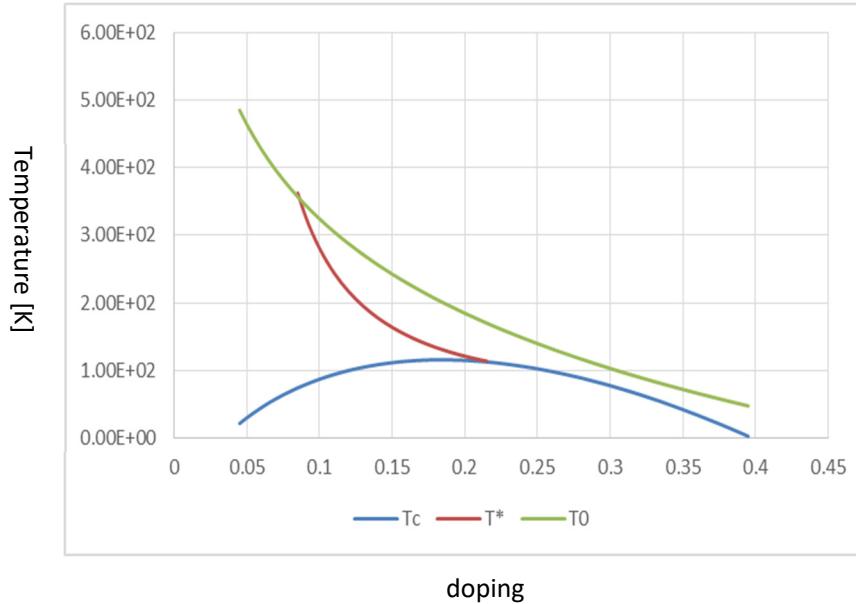
Figure 7. The complete depiction from theoretical calculations of T_c, T^*, and T_0 vs. doping. Note that the horizontal axis is $\frac{N_A}{2n_i}$. For the previous figure of T_c graph, T^* and T_0 are added. Note that T^* is depicted on the understanding that it is smaller than T_0. Moreover, T^* has the gradual and easy minimum point on touching T_c- dome at the doping 0.21. Thus, it does not exist in the T_c-dome. As mentioned, no numerical calculations and fitting methods are employed. T_0 begins with about 500 K and vanishes almost at the same doping at which T_c disappears. As mentioned in the main body, this transition temperature is important when considering the anomaly metal phase.
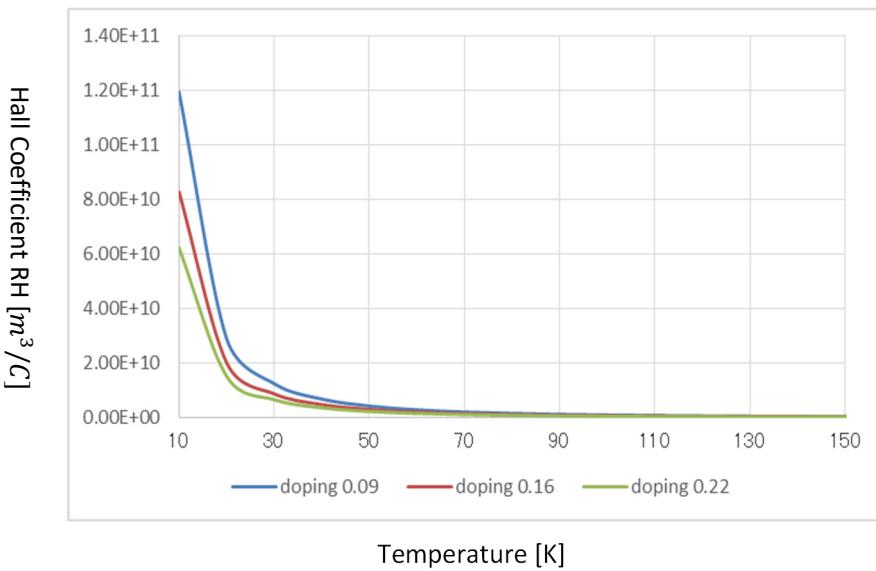
Figure 8. Hall-effect coefficient RH on both temperature and doping. As reported in many experimental papers, lowering the doping dose arises the RH. The calculated values generally agree with experiments (See Ref [33] of the experiment as a reference）.

Because of the statistic equation for the many-body interactions, Figure 10 shows superconductivity state up to a critical temperature ~140 K. In this figure, the state that relative distance ξ_G between two spherical shells (i.e., two macroscopic Bosons) is under 0 indicates the superconductivity state. From the further temperatures higher than this critical temperature, the relative distance ξ_G becomes much larger as a change of non-continuity. Obviously, a transition occurs at ~140 K. This result accurately agrees with the experiments such as [34]. Importantly, in Figure 10, the macroscopic Boson energy U_B (i.e., the magnetic field interaction Equation (29)), at optimum doping, is substituted in our statistic equation. Thus, the many-body interactions in terms of macroscopic Bosons are the reasons why high-T_c cuprates exhibit a considerably higher critical temperature.

Furthermore, Figure 9 shows a result of theoretical calculation for the electron specific heat coefficient. According to the experiments [35,36], the calculation values are valid; moreover, it takes a maximum at a higher doping.
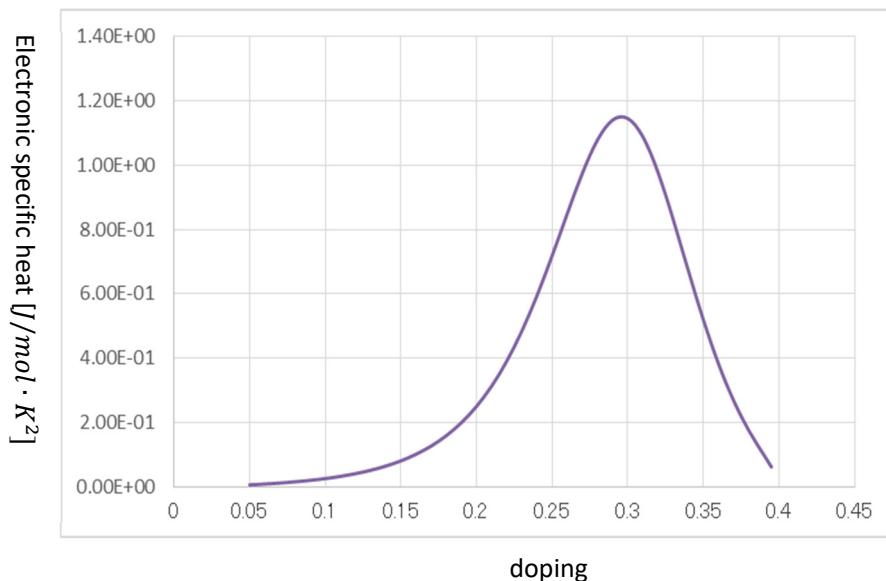
Figure 9. A theoretical result of electron specific heat coefficient on doping. At the relatively high doping, the curve takes the maximum, which agrees with the experiments. In other words, to both lower doping or higher doping from this the maximum, electron specific heat coefficient decreases.
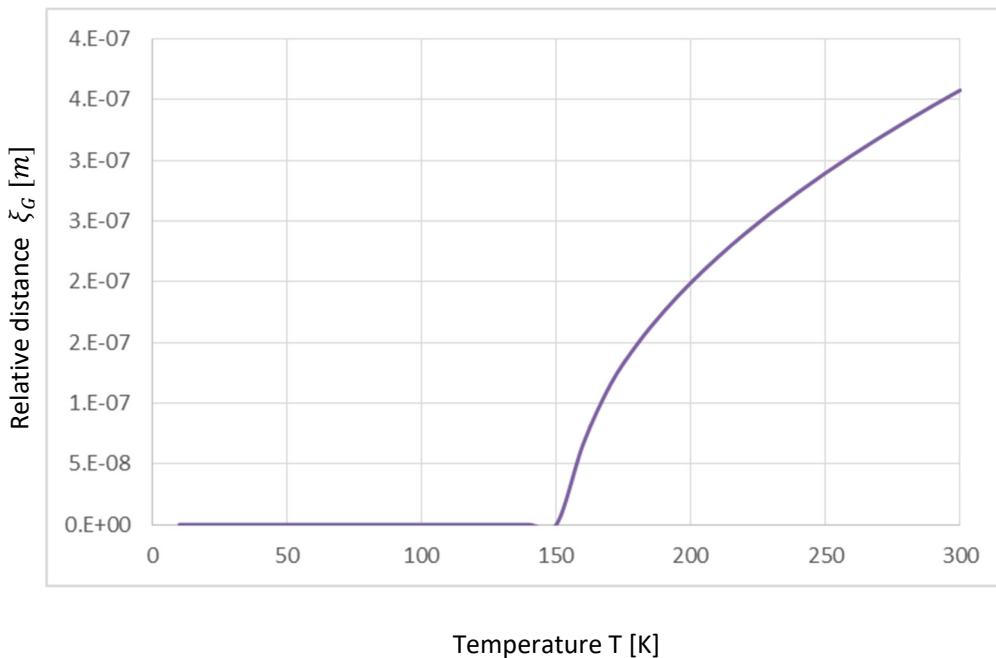
Temperature T [K]

Figure 10. Relative distance between two macroscopic Bosons versus temperature. Because, up to about 140 K, relative distances ξ_G is not defined according to our statistic equation to handle the many-body interactions, the net coherence of two holes is defined as about 1 nm, i.e., superconductivity state is maintained. However, at higher temperatures, relative distances ξ_G suddenly becomes $10^{-7} m$ order. Obviously, a transition occurs at around 140 K. As an important notation, the macroscopic Boson energy U_B is substituted at the optimum doping of 0.16. Thus, the many-body interaction in terms of macroscopic Bosons (not holes) is one of the reasons why high-T$_c$ cuprates exhibit extremely high critical temperatures.

5. Discussion

5.1. Macroscopic Boson and high-T$_c$ Cuprates

We propose a particle describing high-T$_c$ cuprates is not a normal hole but a macroscopic Boson, which is formed by the conservation of angular momentum in 2D and by rotational motion of a hole itself. The concept of a macroscopic Boson, as mentioned, provided a unique partition function; this partition function can explain every property in the anomaly metal phase. Moreover, the presence of this Boson gives substantial reason why high-T$_c$ cuprates have significantly high critical temperature when considered with many-body interactions.

Let us consider how Figure 7 relations each transition to the existence of a macroscopic Boson: In the equation of T_c, considering that the coherence ξ is essentially equal to the radius η of a macroscopic Boson does relation the critical temperature T_c to the macroscopic Boson. Furthermore, to the Equation (38) ($T = -\frac{|\Delta|^2}{k_B^2}\frac{1}{T_c}\frac{1}{\ln\left(\frac{N_A}{n_i}\right)}$), substituting the energy of a macroscopic Boson results in the temperature T^*. Additionally, considering Equation (63) ($n = n_0 \exp\left(-\frac{\mu B_e}{k_B T}\right)$), the value of e^{-1} provides the transition temperature T_0 (i.e., Equation (75)), which implies a creation of macroscopic Boson at that transition temperature.

5.2. Anomaly Metal Phase and Transition Temperature T_0

Thus far, to understand the mechanism of a high-T_c cuprate, it was important to study the source of pseudo-gap energy. Although this is true, another important factor that should be understood is the source of the transition temperature T_0, which defines the anomaly metal phase appearance. As mentioned, all equations that describe the anomaly metal phase have the parameter T_0 and T_c.

5.3. Highlights of the Process for the Materials to Undergo Superconductivity

Let us review the process, which describes the mechanism from forming a macroscopic Bosons to undergoing BE condensation. First, high-T_c cuprate reaches the transition temperature T_0 with a lower or no refrigeration. At this stage, because the wavelength of a hole along c-axis becomes longer than the width of a 2D CuO_2 surface, the net 3D disappears and the conservation of angular momentum forms a macroscopic Boson, which indicates the rotation of a hole producing a magnetic field energy. Thus, this magnetic field energy gives a mass of macroscopic Boson.

By further refrigeration, our established statistic equation results in the following:

1. Many-body interactions, including the magnetic field energy of macroscopic Bosons and Coulomb interactions, result in very short relative distance of two holes (i.e., the net coherence of ~1 nm) as a result of two the sphere shells being superposed. Note that, at this stage, the paring of two macroscopic Bosons indicates the pairing of two holes.

2. Simultaneously, considering the short relative distance, two holes gain a strong combination of the Lorentz force when the relative kinetic energy among two holes becomes 0; note that all Cooper pairs take the identical energy and thus BE condensation is produced, which is the source of the Meissner effect.

Although the derivation of a macroscopic wave function inevitably results in the London equation using the GL equation [37]; herein, let us review the reason why the Meissner effect is derived by another approach, thus stressing the converged and constant phase θ_0.

Under an applied magnetic field *B* (i.e., vector potential *A*), we can derive the Aharonov–Bohm (AB) effect [38] from the initial macroscopic wave function.

$$\psi_A = |\psi| exp[(\theta_0 + \frac{2q}{\hbar} \int Ads)j\},\tag{89}$$

where q, j, and θ_0 denote the hole charge, imaginary unit and converged phase of the macroscopic wave function, respectively.

From Equation (89), it is derived that

$$(\theta_0 + \frac{2q}{\hbar} \int Ads) = 2n\pi,\tag{90}$$

where n is the integer, and considering center-of-mass motion,

$$\theta_0 = 2k_0 x,\tag{91}$$

Substituting Equation (91) in Equation (90) and differentiating both sides of Equation (90), we obtain

$$2k_0 = -\frac{2q}{\hbar}A.\tag{92}$$

The probability density flow is then defined as follows:

$$j_s = q|\psi|^2 \frac{\hbar k_0}{m},\tag{93-1}$$

$$\int |\psi|^2 dv = 1.\tag{93-2}$$

Substituting Equation (92) in Equation (93-1), we derive the following London equation:

$$j_s = -q^2 |\psi|^2 \frac{1}{m}A.\tag{94}$$

This is the identical result from approaches by the GL equation.

5.4. The Reason Why High-T$_c$ Cuprates Have Significantly High Critical Temperature

As mentioned, an attractive force is the Lorentz force when two charged particles have no relative kinetic energy. However, as shown in Figure 11, this concept can be satisfied in s-wave pair and d-wave pair. Considering this schematic, the pair symmetry of high-T$_c$ cuprates is not very important. Rather, it is crucial to focus on an irregular many-body interactions in high-T$_c$ cuprates for an explanation of the significantly high critical temperature.

Paring of s-wave picture

Paring of d-wave picture
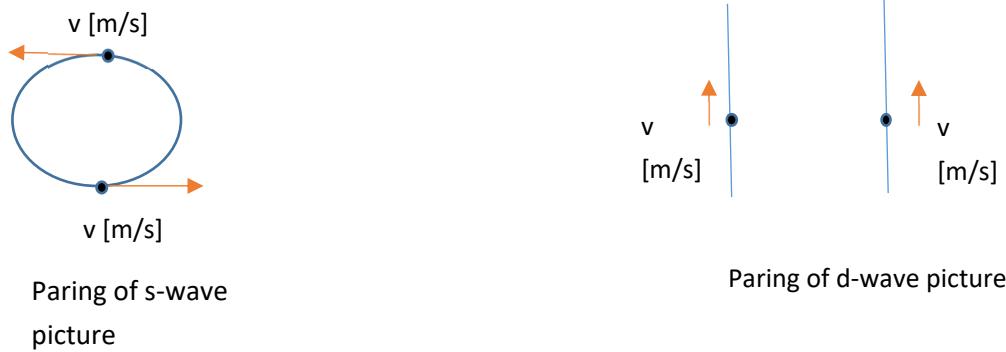
Figure 11. Schematic of paring symmetries. The principle to generate an attractive force between two charged particles is that relative momentum must be equal. That is, when this principle is satisfied and if outer macroscopic heat energy does not disturb, the two charged particles between a long distance are combined by the generated attractive force, which stems from the Lorentz force. The above figure illustrates this principle, i.e., s-wave and d-wave symmetries. This is why there is another irrelevant particle among force–experiencing two particles. This irrelevant charged particle with different momentum does not experience this attractive force. However, the Coulomb interactions does not have this characteristic.

As per the model employed to handle many-body interactions in terms of charged particles, it is normally impossible for two particles to take their relative distance shorter than ~10^{-7} m. In this case, however, our employed equation in many-body interactions has magnetic field interaction U_B in Equation (34) because of the presence of macroscopic Bosons (i.e., pseudo-gap energy) ad Coulomb interactions. Therefore, this fact renders relative distance between two macroscopic Bosons to be almost 0 up to a high temperature, which makes the net coherence of two holes become the order on the cell of a CuO$_2$ surface (i.e., ~1 nm). This fact indicates that the combination energy becomes very strong.

This is demonstrated as shown in Figure 10, which results in a critical temperature of ~140 K. Considering U_B in Equation (34) in our model equation to handle many-body interactions is pseudo-gap energy, Equation (24), which is essentially equal to the mass of a macroscopic Boson, the parameter η [m] (i.e., radius of a Boson and order on a CuO$_2$ cell) determines the critical temperature. As per our derived statistic equation, the larger U_B is, the higher a critical temperature T_c, and actual high-T$_c$ indicates that U_B is sufficiently large, which is caused by the fact that the parameter η [m] is sufficiently small, in addition to optimum doping.

In Equation (34), given the value of 0 for ξ_G, immediately the doping variable becomes fixed and the representative critical temperature $T_{c,\,rep}$ is derived;

$$k_B T_{c,rep} = \frac{2}{3} U_{B,0}, \tag{95}$$

where $U_{B,0}$ indicates the pseudo-gap of Equation (24) for maximum doping. Thus, T_c implies the representative critical temperature.

The calculation of quantities by Equation (95) is shown in Figure 12. In this figure, the horizontal axis implies η of the radius of a macroscopic Boson. This parameter indicates the unit cell order of the CuO$_2$ surface. An important point is that, considering the parameter η is proportional to the lattice constant and although every high-T$_c$ cuprate has macroscopic Bosons, differences in lattice constants

render their critical temperature to be variable. Thus, if the type of material among the high-T_c cuprates differs, then the critical temperature is different.

To conclude, the existence of a macroscopic Boson indicates that:

1) It causes the anomaly metal phase in high-T_c cuprates.
2) Irregular many-body interactions are caused by it, which results in a high critical temperature higher than LN_2.

Note that, if we consider electron-doping in a Mott insulator, carrier concentration dominates over the lattice concentration n_i considering local electrons at each lattice in the Mott insulator; thus, the sign of the function ln in Equation (24) of pseudo-gap energy (i.e., U_B in Equation (34)) is altered. Hence, the sign of U_B in Equation (24) becomes the opposite, which makes electron-doping unable to have a high critical temperature because, on the contrary, U_B would prevent the enhancement of critical temperatures T_c.
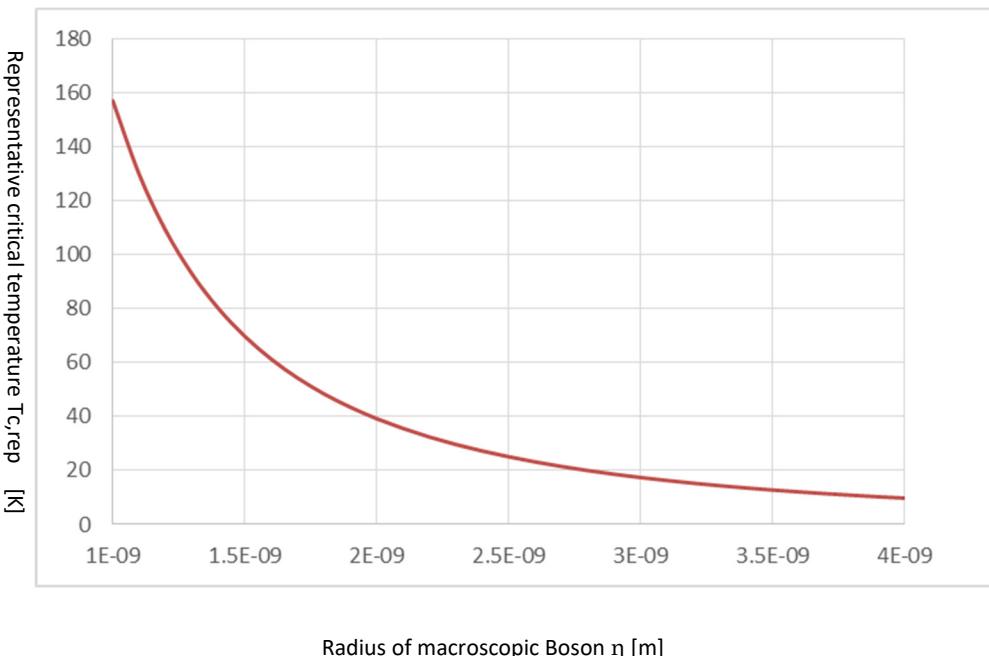
Figure 12. The representative $T_{c,rep}$ for optimum doping vs. the radius of a macroscopic Boson η. Of note, the parameter η depends on a lattice constant. As shown, $T_{c,rep}$ is very sensitive for parameters η. This indicates that, among high-T_c cuprates, varying substances renders their critical temperatures to be variable.

5.5. Image of Cooper Paring of Two Holes When $T \leq T_C$

Figure 13 is an image that a hole on 2D of CuO_2 cell takes a circle, which implies a macroscopic Boson. When two macroscopic Bosons are close to each other and when the relative velocity between the two holes is zero, these two holes take the identical and rotational velocity and take the identical angular frequency as shown in Figure 14. Therefore, when the attractive force principle is satisfied, in which the fact that relative velocity is zero is the source of an attractive force between them, the two holes take rotations, keeping the constant relative distance. This fact is represented in Figure 15. That is, these holes take parallel motions. This corresponds to the d-wave pairing.
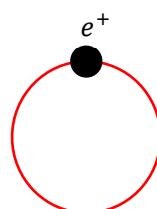
Figure 13. Schematic of a macroscopic Boson.
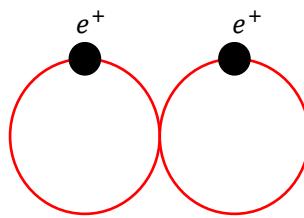
Figure 14. Schematic of paring of two macroscopic Bosons (i.e., the two holes).
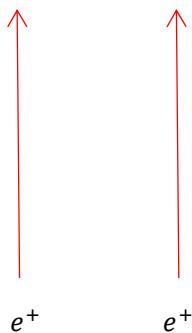
Figure 15. Translation of the aforementioned Figure 14.

5.6. Consideration of Significances in This Paper

We believe that this study is significant because:

1) It clarified why high-T_c cuprates have actual high critical temperature higher than LN_2.
2) It demonstrated that almost puzzles, including the properties of anomaly metal phase reported in previous articles, have been attributed to the presence of a macroscopic Boson.

To date, multiple theoretical investigations were reported to explain the mechanism of high-T_c cuprates but most of them used numerical computing or fitting methods; however, a general understanding of how the mechanism worked was largely unclear. Therefore, we proposed a detailed explanation of the mechanism that has been proposed for a comprehensive understanding of high-T_c cuprates.

Anticipated results and spillover effects:

1) The analytical and physical understanding of high-T_c cuprates described in this study will promote the search for and synthesis of new materials exhibiting higher critical temperature near room temperature than standard materials at any given pressure.
2) All fields of condensed matter physics rely on statistical methods. Therefore, pure analytical (not numerical) approaches can be applied to many-body interactions. Our model that handles many-body interactions will provide new results to unsolved problems in condensed matter physics. For example, the analysis of many-body interactions of magnetic quanta would solve the primary problems of physics and superconducting technologies such as analytical formulation of critical current density.

6. Conclusion

This study described theoretically high-T_c cuprate properties such as the transition temperatures on doping, Hall effect or electron specific heat coefficient on doping. Moreover, it established a novel model to handle general many-body interactions, which explained why the high-T_c cuprates exhibit a significantly high critical temperature.

In general, the derived resultant equations' values accurately agree with data from experimental studies with no numerical calculations and fitting methods.

As discussed in the Discussion, consider the summary of significances in the present study.

1) It has uncovered the source of mysteries in high-T_c cuprates, i.e., the presence of a macroscopic Boson.

2) It has succeeded in describing the anomaly metal phase with a pure theory, which has no fitting or numerical calculations and which agrees with experiments.

3) It has established a new model to handle general many-body interactions; using this model, this study has clarified why high-T_c cuprates have considerably high critical temperatures.

The resistivity on lower doping in the anomaly metal phase is not discussed in this study. However, an equation for conductivity, which takes linearly temperature dependence (i.e., non-linearly resistivity), was obtained in the theoretical section of this study because the carrier concentration in Equation (62), which lineally depends on temperatures, indicates the conductivity. However, this equation employs the critical temperature T_c and thus, over the lower doping, in which the resistivity appears, this equation is not available because, over the lower doping, critical temperatures are not defined. Thus, this will be a natural follow-up.

Moreover, the theory this paper presented seems not to describe electron doping cuprates. Furthermore, very recently, 2-dimentional CDW phases dependent on doping were measured. Thus, it is necessary to research these facts as follow-ups. However, in Appendix B of this paper, a preliminary calculation of the 2-dimensional CDW will be presented.

Acknowledgements: We thank Enago (www.enago.jp) for the English language Review. We appreciate for publishing this study as a preprint in *Preprints* in MDPI: Ishiguri, S. Analytical Descriptions of High-Tc Cuprates by Introducing Rotating Holes and a New Model to Handle Many-Body Interactions. Preprints 2020, 2020050105. https://doi.org/10.20944/preprints202005.0105.v4

Appendix A

Analytical calculations of Curie temperatures considering many-body interactions

Appendix A.1. Introduction

The purpose of this appendix A is to confirm the proposed new model to handle many-body interactions described in the main text by applying another physical phenomenon. For example, we now introduce transitions of ferromagnetic material, i.e., Curie temperature.

Before conducting an actual calculation, we will briefly discuss certain background information to understand the significance of this appendix. Concerning transition phenomena, many studies have been reported. In particular, the Ising model is the most famous and basic. According to our literature review, however, few studies exist, which accurately predicted that the transition temperatures agreed with the experimental data. Moreover, many statistic physics textbooks claim that the Ising model in 2D provides an equation of transition temperature but there is no known model in 3D. If we follow the existing theory, a calculation of transition temperature indicates the evaluation of exchange interaction. However, this interaction is quite abstract and thus it difficult to evaluate in every ferromagnetic material. A general formula to determine a transition temperature has not been obtained because the partition function considering many-body interactions cannot be mathematically calculated.

In this Appendix A, using our established model for many-body interactions, we predict the actual values of transition temperatures, which sufficiently agree with experimental values. These calculations do not involve any numerical calculation or fitting method. Here, we provide a new model for statistical physics considering many-body interactions.

Appendix A.2. Predictions of Curie Temperature Using Our Employed Model to Handle Many-Body Interactions

As shown in Figure A1, a magnetic moment $\vec{\mu}$ is located in the center of a sphere shell dN at which the temperature is T_i. Similar to that of the main text, the following balanced relation holds:

$$\text{(magnetic field interaction from magnetic moments)} = \frac{3}{2}k_B T_i dN \tag{A-1}$$

In this equation, the left-hand side is given as follows:

$$-\vec{\mu}\cdot\vec{B}$$

As every basic text describes, a magnetic field **B** is represented as follows:

$$\vec{B} = -\frac{\mu_0}{4\pi}\left[\frac{\vec{\mu}}{r^3} - \frac{3(\vec{\mu}\cdot\vec{r})\vec{r}}{r^5}\right], \tag{A-2}$$

where **r** is radius of the sphere shell dN.
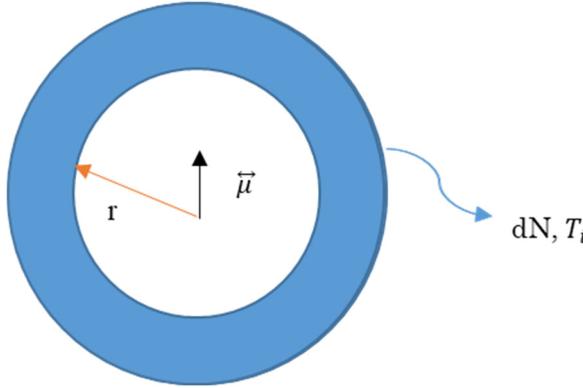
Figure A1. A schematic of our model to apply a ferromagnetic material. Basically, the concept to handle many-body interactions is the same as the case presented in the main text. That is, force of expansion from the central magnetic moment $\vec{\mu}$ is balanced to force of compression from the immediately outer locations, which are equal to kinetic energies in the differential number dN. Note that this case does not include the magnetic field interaction using macroscopic Bosons. Calculating the balanced equation results in a statistic equation that involves many-body interactions.

In this equation, the first term indicates ferromagnetism, while the second term indicates antiferromagnetism. Because the present case is to handle a ferromagnetic material, we employ the first term. Moreover, the directions of two magnetic moments $\vec{\mu}$ are assumed to be parallel, i.e., the scalar product between two $\vec{\mu}$ is positive. Accordingly, the above equation becomes

$$-\vec{\mu}\cdot\left[-\frac{\mu_0}{4\pi}\frac{\vec{\mu}}{r^3}\right] = \frac{3}{2}k_B T_i dN. \tag{A-3}$$

Moreover, as mentioned, dN is expressed as follows considering the volume element of the integral:

$$\frac{\mu_0}{4\pi}|\vec{\mu}|^2\frac{1}{r^3} = \frac{3}{2}k_B T_i dN = \frac{3}{2}k_B T_i \times gf d\vec{k}, \tag{A-4-1}$$

$$d\vec{k} = \frac{1}{dv} = \frac{1}{\frac{4\pi}{3}r^3}. \tag{A-4-2}$$

Thus, an important equation is derived as follows:

$$\mu_0|\vec{\mu}|^2 = \frac{9}{2}k_B T_i gf = \frac{9}{2}k_B T_i g\frac{1}{\exp\left(-\frac{E_i-E_F}{k_B T_i}\right)-1}. \tag{A-5}$$

In this Bose statistic equation, E_i denotes the zero-point energy of phonon, i.e., the Debye temperature and E_F is a chemical potential, which is equal to the Gibbs free energy, but especially in this case implies only an internal energy. Therefore, this chemical potential is derived from electron specific heat coefficient γ as follows:

$$\mu_0|\vec{\mu}|^2 = \frac{9}{2}k_B g\frac{T}{\exp\left[-\frac{1}{k_B T}\left(\frac{3}{2}k_B\theta_D+\gamma T^2\right)\right]-1}. \tag{A-6}$$

In this case, a transition temperature of T_c is assumed to be obtained by considering the extremum from this equation. Hence, to calculate differentials, T_i is considered to be a variable continuous temperature T because there are now no dependent parameters on the index i except T_i. Therefore, the following equation is calculated.

$$\frac{d}{dT}\mu_0|\vec{\mu}|^2 = 0 \ . \tag{A-7}$$

Consequently, the following equation is obtained:

$$\frac{\gamma T^2 - \frac{3}{2}k_B\theta_D}{k_B T} = -1, \tag{A-8-1}$$

$$\mathrm{T} \equiv T_c = -\frac{k_B}{2\gamma} + \sqrt{\frac{3k_B\theta_D}{2\gamma}} \approx \sqrt{\frac{3k_B\theta_D}{2\gamma}}. \tag{A-8-2}$$

Table A1 lists the physical constants of a ferromagnetic metal Fe.

Table A1. Fe physical constants.

Debye temperature θ_D	470 K
Electron specific heat coefficient γ	8.4×10^{-27} J/K^2

Employing these physical constants, the transition temperature T_c for the metal Fe is calculated as follows:

$$T_c \approx 1.08 \times 10^3 \ \mathrm{K} \ . \tag{A-9}$$

Because measurements of the transition report 1043 K, the agreement is sufficient.

Then, we consider the transition temperature of the ferromagnetic Ni. The material Ni has much less thermal conductivity, unlike the metal Fe. This indicates that a chemical energy, i.e., the internal thermal energy is allowed to be ignored. Thus, from Equation (A-8-1), the T_c-equation is simply expressed as follows:

$$\frac{3}{2}k_B\theta_D \approx k_B T_c. \tag{A-10}$$

Because the Debye temperature of Ni is reported as 450 K, T_c is calculated as follows:

$$T_c \approx 675 \ \mathrm{K} \ . \tag{A-11}$$

Compared with a measured transition value 627 K, the agreement can be considered to be sufficient.

Appendix B

A study of 2-dimensional CDW

Appendix B.1. Introduction

Very recently, in the phase diagram in the cuprates, a 2-dimentional Charge Density wave (CDW) transition was found [39]. Although some are mentioning that the recent phase diagram has been more complex, considering the existence of the macroscopic Boson will result relatively easily in the CDW transition. For example, this CDW appears for a parallel magnetic field for the c-axis [40,41], which indirectly implies the existence of a macroscopic Boson. Because of the existence of the macroscopic Boson, now we consider only 2-dimentional CDW. This appendix B would like to derive this CDW transition.

Appendix B.2. Calculations

The CDW is, in short, a stational wave, and thus we employ Figure 3 and its equations in the main body.

The eigenvalue of the stational wave in Figure 3 is again

$$E_i = \frac{1}{2M}\left(\frac{\hbar \pi i}{2a_i}\right)^2. \tag{B-1}$$

Using equation, the following assumption is provided.

$$Mc^2 \equiv k_B T^*, \tag{B-2}$$

where M is the mass of a macroscopic Boson and c is the seed of light.

In this appendix, the parameter a_i is assumed to be

$$a_i \equiv 1.6 \times 10^{-6} \text{m. (B-3)}$$

The above E_i is a merely energy level, different from two energy levels. Thus, as mentioned in the main body, the fine structure constant α is used to derive a gap of the CDW.

$$k_B T_{CDW} \equiv \alpha E_i = \alpha \frac{1}{2} \left(\frac{\hbar i \pi}{2a_i}\right)^2 \left(\frac{k_B T^*}{c^2}\right)^{-1}, \text{ (B-4)}$$

In the above equation,

$$i \equiv N_0, \qquad \text{(B-5)}$$

where

$$N = N_0 f_r.$$

Thus,

$$T_{CDW} = \alpha \frac{1}{2k_B} \left\{ \frac{\pi \hbar}{2a_i} N \left[-\ln \left(\frac{N_A}{n_i}\right) \right]^{+1} \right\}^2 \times \left(\frac{k_B T^*}{c^2}\right)^{-1}. \text{ (B-6)}$$

In this paper, the phase of the CDW is defined as total macroscopic Bosons are condensed on the condition that Equation (B-2) is formed. Thus, $N=1$ is assumed.

In Figure A2, the result is shown, which well agrees with the experiments [39]. Note that the doping of the maximum is 0.12 (i.e., 1/8), which is also agreed [42,43]. Note that, for the method to create this figure, refer to Method section in the main body. Moreover, the result is not a numerical or fitting calculation.

Note that, importantly, in the superconductivity, the total macroscopic Bosons are condensed but the difference in the CDW is the condensation having the condition Equation (B2). This implies that the macroscopic Bosons are condensed in the CDW phase but they do not take a Cooper pair.
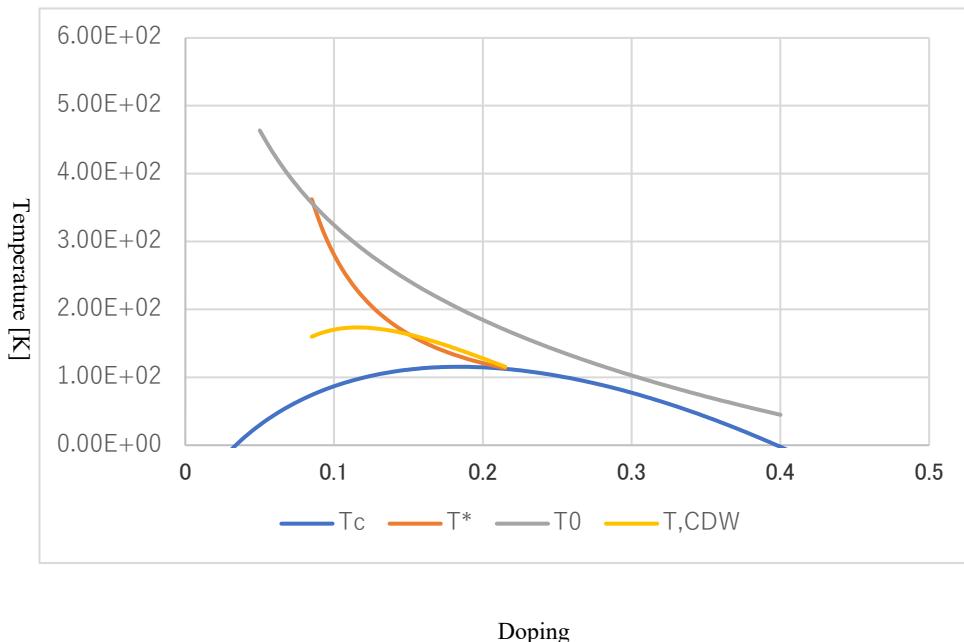
Figure A2. The phase diagram including the 2-dimentional CDW phase. The yellow curve is the transition. This figure was created on the basis of Figure 7 in the man body.

References

1. Ishiguri, S., New attractive-force concept for Cooper pairs and theoretical evaluation of critical temperature and critical-current density in high-temperature superconductors, *Results in Physics*, **3**, 74-79 (2013)

2. Bednorz, J.G. and Müller, K.A., Possible high T_c superconductivity in the Ba-La-Cu-O system, *Zeitschrift für Physik B*. **64**, 189–193 (1986)

3. Yamaguchi, M. et al., A study on performance improvements of HTS coil, *IEEE Trans.Appl. Supercond*. **13** (2), 1848–1851 (2003)

4. Pitel, J. and Kovac, P., Compensation of the radial magnetic field component of solenoids wound with anisotropic Bi(2223)Ag tape, *Supercond. Sci. Technol.* **10** 847 (1997)

5. Ishiguri, S. and Funamoto,T., Performance improvement of a high-temperature superconducting coil by separating and grading the coil edge, *Physica C* **471**, 333–337 (2011)

6. Somayazulu,M. et al., Evidence for Superconductivity above 260 K in Lanthanum Superhydride at Megabar Pressures, *Phys. Rev. Lett*. **122**, 027001 (2019)

7. Zurek, E. and Chem, T. Bi, J., High-temperature superconductivity in alkaline and rare earth polyhydrides at high pressure: A theoretical perspective, *J. Chemical. Phys*. **150**, 050901（2019）.

8. Drozdov, A. P. et al., "Superconductivity at 250 K in lanthanum hydride under high pressures", *Nature* **569**, 528（2019）.

9. Wang, T. et al., Optimal alloying in hydrides: Reaching room-temperature superconductivity in LaH_{10}, *Phys. Rev. B* **105**, 174516（2022）.

10. Pickett, W.E., Pseudopotential methods in condensed matter applications, *Rev. Mod. Phys*. **61**, 433 (1989)

11. Mukuda, H. et al., Uniform Mixing of High-Tc Superconductivity and Antiferromagnetism on a Single CuO_2 Plane of a Hg-Based Five-Layered Cuprate, *Phys. Rev. Lett.*, **96,** 087001 (2006)

12. Basov, D.N. and Timusk, T., Electrodynamics of high-Tc superconductors, *Rev Mod. Phys.*, **77**, 721 (2005)

13. Tacon, M. Le. et al., Two energy scales and two distinct quasiparticle dynamics in the superconducting state of underdoped cuprates, *Nature Physics*, **2**, 537 (2006)

14. Tanaka, K. et al., Distinct Fermi-Momentum-Dependent Energy Gaps in Deeply Underdoped Bi2212, *Science*, **314**, 1910 (2006)

15. Uchida, S. High-T_c cuprates, *Japanese Applied Physics* (institute journal), **80**(5), 383-386 (2013)

16. Fujita, T. High-Tc cuprates, *J. Cryogenics and Superconducting Societies of Japan*, **47**(2), 89-95 (2012)

17. Fischer, Ø. et al., Scanning tunneling spectroscopy of high-temperature superconductors, *Rev. Mod. Phys*. **79**, 353 (2007)

18. Anderson, P. W. et al., The physics behind high-temperature superconducting cuprates: the 'plain vanilla' version of RVB, *J. Phys.: Condens. Matter,* **16**(24), R755 (2004)

19. Ogata, M. and Fukuyama, H., The t–J model for the oxide high-Tc superconductors, *Rep. Prog. Phys.*, **71**, (2008)

20. Scalapino, D.J., The case for $d_{x^2-y^2}$ paring in the cuprate superconductors, *Phys. Rep.*, **250**, 329 (1995)

21. Moriya, T. and Ueda, K., Spin fluctuations and high temperature superconductivity, *Advances in Physics.*, **49**, 555 (2000)

22. Luetkens, H. et al., The electronic phase diagram of the $LaO_{1-x}F_xFeAs$ superconductor, *Nature material*, **8**, 305-309 (2009)

23. Dagotto, E., Correlated electrons in high-temperature superconductors, *Rev. Mod. Phys*. **66**, 763 (1994)

24. Lanzara, A. et al., Evidence for ubiquitous strong electron–phonon coupling in high-temperature superconductors, *Nature* **412,** 510–514 (2001)

25. Pan, S. H. et al., Imaging the effects of individual zinc impurity atoms on superconductivity in $Bi_2Sr_2CaCu_2O_{8+\delta}$, *Nature* **403**, 746–750 (2000)

26. Kohsaka Y. et al., An Intrinsic Bond-Centered Electronic Glass with Unidirectional Domains in Underdoped Cuprates, *Science* **315** (5817),1380-1385 (2007)

27. Fauqé, B. et al., Magnetic Order in the Pseudogap Phase of High-T_c Superconductors, *Phys. Rev. Lett*. **96**, 197001 (2006)

28. Nomura, S., *Introduction of Quantum Mechanics,* 105-106, Corona Publishing co. LTD, Tokyo (2002)

29. Norman, M. R., et al., Destruction of the Fermi surface in underdoped high-Tc superconductors, *Nature* **392**,157–160 (1998)

30. Ishihara, H., *Semiconductor Electronics*, 16, Iwanami Shoten, Tokyo (2002)

31. Chakravarty, S., et al., Interlayer Tunneling and Gap Anisotropy in High-Temperature Superconductors, *Science* **261**(5119), 337-340 (1993)

32. Fukuyama, H. and Akimitsu, J. et al., *Handbook of Superconductors*,143-145, Asakura-Shoten, Tokyo (2010)

33. Ando, Y. et al., Carrier concentrations in $Bi_2Sr_{2-z}La_zCuO_{6+\delta}$ single crystals and their relation to the Hall coefficient and thermopower, *Phys. Rev. B* **63,** 069902 (2001)

34. Gao, L. et al., Study of superconductivity in the Hg-Ba-Ca-Cu-O system. *Physica C,* **213**(3-4), 261-265 (1993)

35. Loram, J. W. et al., A systematic study of the specific heat anomaly in $La_{2-x}Sr_xCuO_4$. *Physica C* **162-164**, 498 (1989)

36. Momono, N. et al., Low-temperature electronic specific heat of $La_{2-x}Sr_xCuO_4$ and $La_{2-x}Sr_xCu_{1-y}Zn_yO_4$. Evidence for a d wave superconductor, *Physica C* **233**, 395 (1994)

37. Kittel,C., Introduction to Solid State Physics (Japanese 8th-edition), Appendix I, Maruzen, Tokyo (2010)

38. Aharonov, Y. and Bohm, D., Significance of Electromagnetic Potentials in the Quantum Theory, *Phys. Rev.* **115**, 485 (1959)

39. Matsumura, S. et al., 72th the physical Society of Japan (conference abstract), 20aL42-11 (2017)

40. Wu, T. et al., Magnetic-field-induced charge-stripe order in the high-temperature superconductor $YBa_2Cu_3O_y$, *Nature* **477**, 191 (2011)

41. Wu, T. et al., Emergence of charge order from the vortex state of a high-temperature superconductor, *Nature Communication* **4**, 2113 (2013)

42. Ghiringhelli, G. et al., Long-Range Incommensurate Charge Fluctuations in $(Y,Nd)Ba_2Cu_3O_{6+x}$, *Science* **337**, 821 (2012)

43. Chang, J. et al., Direct observation of competition between superconductivity and charge density wave order in $YBa_2Cu_3O_{6.67}$, *Nature Physics* **8**, 871 (2012)